Journal of Nuclear Medicine, published on February 2, 2023 as doi:10.2967/jnumed.122.264597

Signaling Network Response to Alpha-Particle Targeted Therapy with Actinium-225 Labeled Minigastrin Analogue ^{225}Ac-PP-F11N Reveals Radiosensitizing Potential of HDAC Inhibitors

Yun Qin [1,2], Stefan Imobersteg [1], Stephan Frank [3], Alain Blanc [1], Tanja Chiorazzo [1], Philipp Berger [4], Roger Schibli [1,2], Martin P. Béhé [1#] and Michal Grzmil [1#]

[1] *Center for Radiopharmaceutical Sciences, Paul Scherrer Institute, Villigen, Switzerland*
[2] *Department of Chemistry and Applied Biosciences, ETH Zurich, Switzerland*
[3] *Division of Neuropathology, Institute of Pathology, University of Basel, Switzerland*
[4] *Laboratory of Nanoscale Biology, Paul Scherrer Institute, Villigen, Switzerland*

[#] Correspondence to: Martin P. Béhé (martin.behe@psi.ch), phone: +41 56 310 28 17 and Michal Grzmil (michal.grzmil@psi.ch), phone: +41 56 310 28 57

This research was funded by the Swiss Cancer League (KFS-3960-08-2016-R) to M.G., M.B. and R.S.

Word count: 4982

Running title: Signaling Network Response to TAT

ABSTRACT

Alpha-particle emitters have recently been explored as valuable therapeutic radionuclides. Yet, toxicity to healthy organs and cancer radioresistance limit the efficacy of targeted alpha-particle therapy (TAT). Identification of the radiation-activated mechanisms, which drive cancer cell survival, provides opportunities to develop new points for therapeutic interference to improve efficacy and safety of TAT. **Methods:** Quantitative phosphoproteomics and matching proteomics followed by the bioinformatics analysis were employed to identify alterations in the signaling networks in response to TAT with actinium-225 labeled minigastrin analogue ^{225}Ac-PP-F11N in A431 cells, which overexpress cholecystokinin B receptor (CCKBR). Western blot (WB) analysis and microscopy verified the activation of the selected signaling pathways. Small-molecule inhibitors were used to validate the potential of the radio-sensitizing combinatory treatments both *in vitro* and in A431/CCKBR tumor-bearing nude mice. **Results:** TAT-induced alterations involved in DNA damage response (DDR), cell cycle regulation, signal transduction as well as RNA transcription and processing, cell morphology and transport. WB analysis and microscopy confirmed increased phosphorylations of the key proteins involved in DDR and carcinogenesis including P53, P53BP1 histone deacetylases (HDACs) and H2AX. Inhibition of HDAC class II, ataxia-telangiectasia mutated (ATM) and p38 kinases by TMP269, AZD1390 and SB202190, respectively, sensitized A431/CCKBR cells to ^{225}Ac-PP-F11N. Combination of ^{225}Ac-PP-F11N with HDAC inhibitor vorinostat (SAHA) showed significantly reduced viability and increased DNA damage of A431/CCKBR cells as well as the most pronounced tumor growth inhibition and the extended mean survival of A431/CCKBR xenografted nude mice as compared to the control and monotherapies. **Conclusions:** Our study revealed the cellular responses to TAT and demonstrated the radiosensitizing potential of HDAC inhibitors to ^{225}Ac-PP-F11N in CCKBR-positive tumors. This proof-of-concept study recommends development of the novel radiosensitizing strategies by targeting TAT-activated and survival-promoting signaling pathways.

Key Words: Actinium-225, Phosphoproteomics, Minigastrin, CCKBR, Radioresistance

INTRODUCTION

Targeted radionuclide therapy (TRT) delivers cytotoxic radionuclides to cancer lesions and shows promise for the treatment of patients with unresectable metastatic cancers (*1*). In 2018, FDA approved lutathera (lutetium-177 labeled dotatate peptide) for the first-in-class peptide receptor radionuclide therapy (PRRT) of somatostatin receptor-positive gastroenteropancreatic and neuroendocrine tumors and more recently, lutetium-177-labeled prostate-specific membrane antigen (PSMA) ligand [^{177}Lu]Lu-PSMA-617 (Pluvicto) has been approved for the treatment of PSMA-positive metastatic castration-resistant prostate cancer patients (*2,3*). To improve therapeutic efficacy, previous studies employed alpha emitters such as actinium-225, with high linear energy transfer (LET) and a low tissue penetrating range (40−100 μm) (*4*). Despite promising therapeutic outcomes the effectiveness of targeted alpha-particle therapy (TAT) requires further optimization due to the impaired life quality of treated patients (*5*). Understanding the responses of cancer cells to TAT would allow the development of radiosensitization strategies with improved therapeutic efficacy at lower activities and reduced side effects. We have recently developed ^{225}Ac-labeled minigastrin analogue ^{225}Ac-PP-F11N, which targets overexpressed cholecystokinin B receptor (CCKBR) in various human cancers including medullary thyroid, ovarian, and small-cell lung cancer (SCLC), as well as gliomas (*6*). In a pilot and a phase I study (NCT02088645), ^{177}Lu-PP-F11N demonstrated medullary thyroid cancer (MTC)-specific accumulation and low retention in kidney and bone marrow, whereas the median tumor-to-stomach dose ratio of 3.34 indicated stomach as a potential dose-limiting organ (*7*). In order to understand cellular responses to ionizing irradiation caused by alpha-particle emitting radiolabeled minigastrin, and to further develop concomitant radiosensitizing strategies, we analyzed signaling networks in response to ^{225}Ac-PP-F11N in A431/CCKBR cells by quantitative phosphoproteomics and corresponding proteomics analysis. This study translates acquired basic radiobiology knowledge into novel treatment opportunities and provides proof-of-concept for the development of radiosensitizing strategies for TRTs.

MATERIAL AND METHODS

Reagents and Radiolabeling

Selective inhibitors; AZD1390 (ATM), TMP269 (class IIa HDAC), SB202190 (p38α and p38β2) and SAHA (class II, III and IV HDAC) were obtained from Lucerna-Chem. Actinium-225 (in 0.1 M HCl) was purchased from ITG GmbH, whereas N-terminal DOTA-conjugated gastrin analogue PP-F11N (DOTA-$(DGlu)_6$-Ala-Tyr-Gly-Trp-Nle-Asp-Phe) was from PSL GmbH. Radiolabeling and separation of ^{225}Ac-PP-F11N are described in the supplemental material (*6*).

Cell Culture and Proliferation Assay

Human squamous carcinoma A431 cells, which overexpress CCKBR, were kindly provided by Dr. Luigi Aloj (*8*) and cultured at standard condition, and the cell proliferation was analyzed by using the CellTiter 96 AQueous Non-Radioactive Cell Proliferation Kit (Promega) according to the manufacturer's instruction as described in the supplemental material.

Proteomics, Phosphoproteomics and Bioinformatics

Preparation of tryptic peptides and phosphopeptide enrichment, liquid chromatography-mass spectrometry analysis followed by the protein and phosphopeptide identification, and label-free quantification followed by bioinformatics are described in the supplemental material (9).

Western Blot and Immunocytochemistry

For the analysis of protein level and phosphorylation, cells were subjected to Western blot (WB) analysis and immunocytochemistry as described in the supplemental material.

In Vivo Therapy Study

All experiments involving mice complied with Swiss Animal Protection Laws and were approved by the Cantonal Committee of Animal Experimentation (License No. 75699, 2017). The immunocompromised CD-1 female nude mice (Charles Rivers) were implanted with 5 million A431/CCKBR cells via subcutaneous injection. Seven days after inoculation, the nude mice carrying A431/CCKBR tumors were randomly grouped (the average tumor volume per group was 0.13 cm^3, range 0.11-0.14 cm^3) and received 10 daily doses of 50 mg/kg SAHA (dissolved in DMSO/PEG400/Tween80/Saline (10:40:5:45)) or vehicle control via intraperitoneal injection. SAHA dose was selected based on the previous animal studies, which show anti-tumor activity without detectable toxicity (*10*). On the second day of the treatment, one dose of 30 kBq ^{225}Ac-PP-F11N dissolved in 100 µL PBS, or PBS alone as vehicle control, was injected intravenously. Tumor diameter, animal weight, and well-being were recorded at least three times a week and the tumor volume was calculated using the formula $V = (W^2 \times L)/2$. Mice were sacrificed when the tumor reached end-point volume (>1.5 cm^3). Mice with ulcerated tumors, found randomly in all groups, were sacrificed prematurely and were excluded from the study. For the histopathological assessment, *post mortem* dissected stomach and kidney were formalin-fixed, dehydrated and paraffin-embedded for the preparation of Hematoxylin-Eosin (HE) stained tissue sections as described previously (*11*). The image analysis and documentation were performed by using a slide scanner (Nikon Instruments Europe).

Statistics

Nonparametric Mann Whitney unpaired test and Bliss Independence model were used for *in vitro* treatments and calculations of combination index (CI). *In vivo*, one-way ANOVA followed by Tukey's multiple comparison tests were performed for three or more groups using GraphPad Prism 7.00 for Windows 10. For survival analysis, the Gehan-Breslow-Wilcoxon test was performed. Values of $p<0.05$ were considered statistically significant.

RESULTS

Signaling Network Changes in Response to TAT with ^{225}Ac-PP-F11N

We performed quantitative phosphoproteomics and proteomics analysis of the protein lysates derived from the control and ^{225}Ac-PP-F11N-treated A431/CCKBR cells, to identify the molecular changes in response to actinium-225 labeled minigastrin analogue. Phosphoproteomics quantified the abundance of 8952 phosphopeptides, whereas matching proteomics quantified 4250 protein groups (Fig. 1A). The phosphoproteomics and proteomics analysis identified 342 phosphopeptides (Supplemental Table 1 and 2) and 3 proteins (Supplemental Table 3), respectively, with significantly altered abundance in the ^{225}Ac-PP-F11N-treated cells as compared to control cells. Bioinformatics analysis using the STRING platform identified the interaction networks among the proteins with altered levels of phosphorylation in the ^{225}Ac-PP-F11N-treated cells (Fig. 1B). The increased phosphorylation of HDAC9/4/5 at S246/S259/S220, P53BP1 at S1778 as well as P53 at S15 was validated by WB analysis using phospho-specific antibodies (Fig. 1C). Total protein level of 53BP1 and housekeeping protein GAPDH showed no significant difference. Further bioinformatics analysis using DAVID web-based platform identified enriched fold for the biological processes including DNA damage response, cell cycle regulation, signal transduction pathways (Table 1) as well as RNA transcription and processing, cell morphology and adhesion, protein modifications and transport (Supplemental Table 4).

Targeting TAT-Induced Pathways Sensitizes Cancer Cells to ^{225}Ac-PP-F11N

We investigated inhibition of ^{225}Ac-PP-F11N-activated signaling pathways to explore novel strategies for radiosensitization of TAT, previously reported to be associated with radioresistance or survival. We selected three druggable pathways HDAC class II, ATM and p38, which can be targeted by commercially available selective small-molecule inhibitors TMP269, AZD1390, and SB202190, respectively. For the combinatory treatments, the optimal concentration of the inhibitors was determined in A431/CCKBR cells, whereby 5 µM of TMP269, AZD1390, and 2 µM

of SB202190 reduced cell proliferation to 69-89 % of control (Supplemental Fig. 1). Concomitant treatment of A431/CCKBR cells with different doses of ^{225}Ac-PP-F11N and TMP269, AZD1390 or SB202190 reduced cell proliferation to 63-23, 14-8 or 32-23 % of control, respectively, and was significantly lower ($p < 0.05$) as compared to the monotherapy with ^{225}Ac-PP-F11N or inhibitor alone (Fig. 2A-C). The combination of ^{225}Ac-PP-F11N with TMP269 showed a synergistic effect (CI: 0.62-0.85), whereas moderate synergistic and additive effects were obtained for SB202190 and AZD1390 with CI between 0.81-0.99 and 0.96-0.98, respectively. The inhibitions of HDAC9/4/5 phosphorylation at S246/S259/S220 and P53 at S15 as well as P53BP1 at S1778 in response to TMP269 and AZD1390 treatment, respectively, were determined by WB analysis in ^{225}Ac-PP-F11N-treated cells (Fig. 2D).

HDAC Inhibitor SAHA Improves Therapeutic Efficacy of ^{225}Ac-PP-F11N

In a search for novel radiosensitizing approaches for ^{225}Ac-PP-F11N, we selected FDA-approved HDAC inhibitor, suberoylanilide hydroxamic acid (SAHA), which inhibited cell proliferation to 74 % of control at 2 µM (Supplemental Fig. 1). We analyzed DNA double-strand break marker γH2AX (H2AX phosphorylation at S139) to investigate effects on the DNA damage, which expression correlated with the response to TRT (*12*). Combination of ^{225}Ac-PP-F11N and SAHA showed significantly increased speckle number and intensity of the γH2AX in the nucleus (Fig. 3A-C) and reduced A431/CCKBR cell viability (Supplemental Fig. 2) as compared to the monotherapies and control. A431/CCKBR-tumor-bearing nude mice were analyzed after administration of one dose daily for 10 days of 50 mg/kg SAHA alone or in combination with one dose of 30 kBq of ^{225}Ac-PP-F11N. All treatments delayed tumor growth (Fig. 4A). The first mouse reached the endpoint in the control group on day 13 after ^{225}Ac-PP-F11N application, and the average tumor volumes in ^{225}Ac-PP-F11N and combinatorial treatment groups were significantly reduced to 0.46 cm^3 (p=0.04) and 0.36 cm^3 (p=0.02), respectively, as compared to control (0.90 cm^3). Treatment with SAHA reduced average tumor volume to 0.55 cm3 (p=0.12). The mean survival of mice treated with SAHA and

^{225}Ac-PP-F11N was significantly extended (33 days; p=0.04) as compared to the control (22 days) (Fig. 4B and 4C). In contrast, monotherapies with ^{225}Ac-PP-F11N or SAHA extended mean survival to 28 and 25 days, respectively, but these results did not reach statistical significance. To investigate potential toxicity to healthy organs, we analyzed the kidney, involved in circulating radiopeptide excretion, and the stomach, the latter accumulating ^{225}Ac-PP-F11N due to endogenous CCKBR expression (*6*). Histopathological assessment of the kidney and stomach tissue sections from mice treated with SAHA and [^{255}Ac]Ac-PP-F11N did not show any differences as compared to controls (3 mice per group) (Fig. 5). Furthermore, during therapy, no body weight loss was observed in any treatment group (Supplemental Fig. 3).

DISCUSSION

Despite new advances in TAT, cancer radioresistance remains a challenge that worsens therapeutic outcomes in the clinic (*13,14*). In order to identify radiosensitizing molecular targets and to develop combinatory treatments we characterized changes in the cancer signaling network in response to PRRT with Actinium-225 labeled minigastrin analogue ^{225}Ac-PP-F11N. Understanding cancer cell responses can result in the coherent design of radiosensitization strategies to improve the therapeutic window and reduce applied activity, and thus, minimize adverse effects. This rational approach can be also applied to other radioconjugates to develop safer and more efficacious cancer treatments. Our phosphoproteomic analysis identified phosphorylation changes in proteins involved in DNA damage response (DDR), repair and nucleus structure as well as in cell cycle regulation, RNA processing, and signal transduction. Consistently, ionizing radiation leads to the formation of DNA damage foci and activation of DDR pathways via activation of ataxia-telangiectasia mutated (ATM)/checkpoint kinase 2 (Chk2) and ATM- and Rad3-related (ATR)/checkpoint kinase 1 (Chk1), which regulate proteins involved in DNA repair, cell cycle progression as well as chromatin regulation and gene expression (*1*). Although MS-based quantitative characterization of the proteome and post-translational

modifications were previously used in the prediction of drug responses (*15*), identification of cancer biomarkers and sensitization targets for external beam radiation therapy (EBRT) (*16,17*), little is known about cancer responses to targeted radionuclide therapy. Recently, MS-based phosphoproteomics analyzed altered signaling networks in response to targeted radioligand therapy with lutetium-177 and actinium-255 labeled PSMA in a prostate cancer mouse model (*18*). Similarly, the study identified alterations in DNA damage and replication stress response as well as in p53 pathways and suggests that the identified pathways may mediate radioresistance, yet the validation and development of radiosensitizing strategies await further investigation. Despite similarities in the response to TRT, genetic heterogeneity of various cancers influence activation of the signaling pathways and thus, effective radiosensitization might require development of the cancer-type-specific strategies. Among identified alterations, our validation study confirmed increased phosphorylation of HDAC9/4/5 at S246/S259/S220, as well as P53BP1 at S1778 and P53 at S15 in response to ^{225}Ac-PP-F11N. HDACs play a role in the chromatin remodeling and regulation of post-transcriptional gene expression, which are essential processes in DDR (*19*). The phosphorylation of HDAC regulates nucleo-cytoplasmic shuttling, complex formation, and the catalytic activity (*20,21*). Notably, Biade *et al*. reported chromatin conformation changes after co-treatment with HDAC inhibitor Trichostatin A and EBRT, which led to enhanced radiation sensitivity in intrinsically radioresistant colon carcinoma cells (*22*). Consistently in our study, the combination of HDACi with TAT resulted in a synergistic effect on cell viability inhibition, which could be explained by the enhanced number of DNA double-strand breaks. In addition, the chromatin modulators including demethylating agents and HDAC inhibitors were reported to upregulate SSTR2 expression and thus, increased tumor uptake of the radiolabeled octreotide in neuroendocrine and prostate cancer cells (*23*). An assessment of whether these findings also apply to other targeted receptors, including the CCKBR, requires further investigation. The ATM-phosphorylated P53 binding protein 1 (P53BP1) acts as a sensor protein of DNA damages and it is involved in recruiting repair proteins to the damaged chromatin (*24*). The interaction of P53BP1

with the telomere-associated protein RIF1 potentiated cell survival after multi-fractionated radiotherapy and this survival benefit can be revoked by P53BP1 inhibition (*25*). Furthermore, the elevated phosphorylation level of the tumor suppressor P53 on serine-15 after ionizing radiation has been reported to mediate cell growth arrest, which provides time to facilitate DNA repair (*26,27*). Our phosphoproteomics identified increased phosphorylation of MAPK14 (p38 isoform α), which signaling regulates various biological responses including proliferation, differentiation, migration, inflammation as well as stress responses, and survival (*28-30*). Notably, Rac1-mediated p38 activation in response to γ-rays supported cervical carcinoma cell survival and the inhibition of Rac1 activity abrogated the radioresistance conferred by Rac1/p38 activation and significantly enhanced apoptosis (*31*). Thus, previously reported important roles of the HDACs, ATM/P53, and p38 pathways in DDR and survival as well as identified by our study increased phosphorylations in response to TAT points them to potential radiosensitizing targets. Indeed, in the present study inhibition of the HDAC class II, ATM and p38 pathways by small-molecule inhibitors significantly enhanced the cytotoxic effect of ^{225}Ac-PP-F11N in CCKBR-positive cells. As expected, interference with DDR pathways by ATMi AZD1390 sensitized cancer cells to ionizing radiation, whereas p38i showed a weaker radiosensitizing effect than HDACi, which showed the synergistic effect with ^{225}Ac-PP-F11N. Thus, in a search for the most efficient radiosensitizing strategy for clinical applications, we selected for *in vivo* validation HDAC inhibitor, suberoylanilide hydroxamic acid (SAHA, vorinostat), which is approved by the FDA for the treatment of cutaneous T-cell lymphoma patients (*32*). In addition, SAHA showed better anti-cancer activity as compared to other HDAC inhibitor TMP269, and significantly enhanced DNA damage and cytotoxicity of ^{225}Ac-PP-F11N in our *in vitro* assays. As compared to the mono-treatment and control groups, SAHA in combination with ^{225}Ac-PP-F11N produced the most effective therapeutic response *in vivo*. This first proof-of-concept study confirms the radiosensitizing potential of HDAC inhibitors, yet to maximize therapeutic response this study requires further optimization. In agreement with our results, the radiosensitization effects of the HDACi were previously reported in various cancer

models (*19*), and more recently co-treatment with vorinostat improved response to radiolabeled peptide ligand [^{212}Pb]Pb-DOTA-MC1L in mice bearing human melanoma xenografts (*33*). Furthermore, in human RT112 bladder cancer xenografted CD1-nude mice radiotherapy in combination with HDACi panobinostat led to cancer growth delay without a significant increase in the acute and short-term normal tissue radiation toxicity (*34*). Similarly, in our study neither acute radiation toxicity to the kidney or stomach nor significant body weight losses were identified in the mice, which received combinatory treatment, indicating that applied doses of ^{225}Ac-PP-F11N and SAHA were relatively safe and well-tolerated. Moreover, the combination of vorinostat with external radiotherapy has recently entered clinical trials with non-small cell lung cancer (NCT00821951) and glioblastoma (NCT03426891) patients for the safety, tolerability, and efficacy assessment, and thus, it suggests HDACi treatment as a clinically feasible radiosensitizing strategy for TAT in cancer patients.

CONCLUSION

Our phosphoproteomic analysis followed by the validation study revealed alterations in the signaling networks and identified radiosensitizing molecular targets including HDAC, ATM, and p38 in response to TAT with Actinium-225 labeled minigastrin analogue in CCKBR-positive cancer cells. In this study, the explored radiobiology was used to verify new radiosensitizing strategies based on the targeting radiation-activated and survival-supporting pathways. Combination of ^{225}Ac-PP-F11N with HDACi vorinostat enhanced DNA damage and cancer cell cytotoxicity as well as improved therapeutic efficacy in A431/CCKBR-tumor-bearing nude mice. Our proof-of-concept study indicates HDACi treatment as an effective radiosensitization strategy for ^{225}Ac-PP-F11N and further recommends phosphoproteomics for the identification of novel radiosensitizing targets.

DISCLOSURE

This research was supported by the Swiss Cancer Research foundation (KFS-3960-08-2016-R) to M.G, R.S. and M.B. M.B. and R.S. are inventors of the patent WO2015/067473: Mini-gastrin analogue, in particular for use in CCK2 receptor positive tumor, diagnosis and/or treatment. No other potential conflicts of interest relevant to this article exist.

ACKNOWLEDGEMENTS

The authors thank the Functional Genomic Center Zürich (FGCZ) for proteomics and phosphoproteomics service and support.

KEY POINTS

QUESTION: How do cancer cells respond to TAT and which survival-supporting pathways are potential molecular targets for the rational development of radiosensitizing strategies?

PERTINENT FINDINGS: In the response to TAT with [^{255}Ac]Ac-PP-F11N cancer cells induced DDR, cell cycle regulation, RNA transcription and processing as well as signal transduction pathways. Targeting of identified HDAC, ATM, and p38 pathways shows radiosensitizing potential in cancer cells, and clinically approved HDACi vorinostat (SAHA) significantly improves the efficacy of TAT *in vivo*.

IMPLICATIONS FOR PATIENT CARE: Patients with CCKBR-positive tumors could benefit from the combinatory treatment with HDACi and radioactive minigastrin analogue due to enhanced radiosensitivity and anti-cancer activity of HDACi.

References

1. Grzmil M, Meisel A, Behé M, Schibli R. An Overview of Targeted Radiotherapy. In: Lewis JS, Windhorst AD, Zeglis BM, eds. *Radiopharmaceutical Chemistry*. Cham: Springer International Publishing; 2019:85-100.

2. Hennrich U, Kopka K. Lutathera®: The First FDA- and EMA-Approved Radiopharmaceutical for Peptide Receptor Radionuclide Therapy. *Pharmaceuticals (Basel)*. 2019;12:114.

3. FDA Approves Pluvicto/Locametz for Metastatic Castration-Resistant Prostate Cancer. *J Nucl Med.* 2022;63:13N.

4. Poty S, Francesconi LC, McDevitt MR, Morris MJ, Lewis JS. alpha-Emitters for Radiotherapy: From Basic Radiochemistry to Clinical Studies-Part 1. *J Nucl Med.* 2018;59:878-884.

5. Kratochwil C, Bruchertseifer F, Giesel FL, et al. 225Ac-PSMA-617 for PSMA-Targeted α-Radiation Therapy of Metastatic Castration-Resistant Prostate Cancer. *J Nucl Med.* 2016;57:1941-1944.

6. Qin Y, Imobersteg S, Blanc A, et al. Evaluation of Actinium-225 Labeled Minigastrin Analogue [(225)Ac]Ac-DOTA-PP-F11N for Targeted Alpha Particle Therapy. *Pharmaceutics.* 2020;12:1088.

7. Rottenburger C, Nicolas GP, McDougall L, et al. Cholecystokinin 2 Receptor Agonist (177)Lu-PP-F11N for Radionuclide Therapy of Medullary Thyroid Carcinoma: Results of the Lumed Phase 0a Study. *J Nucl Med.* 2020;61:520-526.

8. Aloj L, Caraco C, Panico M, et al. In vitro and in vivo evaluation of 111In-DTPAGlu-G-CCK8 for cholecystokinin-B receptor imaging. *J Nucl Med.* 2004;45:485-494.

9. Deutsch EW, Bandeira N, Sharma V, et al. The ProteomeXchange consortium in 2020: enabling 'big data' approaches in proteomics. *Nucleic Acids Res*. 2020;48:D1145-D1152.

10. Butler LM, Agus DB, Scher HI, et al. Suberoylanilide hydroxamic acid, an inhibitor of histone deacetylase, suppresses the growth of prostate cancer cells in vitro and in vivo. *Cancer Res.* 2000;60:5165-5170.

11. Grzmil M, Qin Y, Schleuniger C, et al. Pharmacological inhibition of mTORC1 increases CCKBR-specific tumor uptake of radiolabeled minigastrin analogue [(177)Lu]Lu-PP-F11N. *Theranostics.* 2020;10:10861-10873.

12. Graf F, Fahrer J, Maus S, et al. DNA double strand breaks as predictor of efficacy of the alpha-particle emitter Ac-225 and the electron emitter Lu-177 for somatostatin receptor targeted radiotherapy. *PLoS One*. 2014;9:e88239.

13. Sgouros G, Bodei L, McDevitt MR, Nedrow JR. Radiopharmaceutical therapy in cancer: clinical advances and challenges. *Nat Rev Drug Discov.* 2020;19:589-608.

14. Gill MR, Falzone N, Du Y, Vallis KA. Targeted radionuclide therapy in combined-modality regimens. *Lancet Oncol.* 2017;18:e414-e423.

15. Frejno M, Meng C, Ruprecht B, et al. Proteome activity landscapes of tumor cell lines determine drug responses. *Nat Commun.* 2020;11:3639.

16. Nader JS, Boissard A, Henry C, et al. Cross-Species Proteomics Identifies CAPG and SBP1 as Crucial Invasiveness Biomarkers in Rat and Human Malignant Mesothelioma. *Cancers (Basel).* 2020;12:2430.

17. Wiechmann S, Saupp E, Schilling D, et al. Radiosensitization by Kinase Inhibition Revealed by Phosphoproteomic Analysis of Pancreatic Cancer Cells. *Mol Cell Proteomics.* 2020;19:1649-1663.

18. Stuparu AD, Capri JR, Meyer CAL, et al. Mechanisms of Resistance to Prostate-Specific Membrane Antigen-Targeted Radioligand Therapy in a Mouse Model of Prostate Cancer. *J Nucl Med.* 2021;62:989-995.

19. Karagiannis TC, El-Osta A. Modulation of cellular radiation responses by histone deacetylase inhibitors. *Oncogene.* 2006;25:3885-3893.

20. Parra M. Class IIa HDACs - new insights into their functions in physiology and pathology. *FEBS J.* 2015;282:1736-1744.

21. Hanigan TW, Aboukhatwa SM, Taha TY, Frasor J, Petukhov PA. Divergent JNK Phosphorylation of HDAC3 in Triple-Negative Breast Cancer Cells Determines HDAC Inhibitor Binding and Selectivity. *Cell Chem Biol.* 2017;24:1356-1367 e1358.

22. Biade S, Stobbe CC, Boyd JT, Chapman JD. Chemical agents that promote chromatin compaction radiosensitize tumour cells. *Int J Radiat Biol.* 2001;77:1033-1042.

23. Adant S, Shah GM, Beauregard JM. Combination treatments to enhance peptide receptor radionuclide therapy of neuroendocrine tumours. *Eur J Nucl Med Mol Imaging.* 2020;47:907-921.

24. Panier S, Boulton SJ. Double-strand break repair: 53BP1 comes into focus. *Nat Rev Mol Cell Biol.* 2014;15:7-18.

25. Eke I, Zong D, Aryankalayil MJ, et al. 53BP1/RIF1 signaling promotes cell survival after multifractionated radiotherapy. *Nucleic Acids Res.* 2020;48:1314-1326.

26. Canman CE, Lim DS, Cimprich KA, et al. Activation of the ATM kinase by ionizing radiation and phosphorylation of p53. *Science.* 1998;281:1677-1679.

27. Fei P, El-Deiry WS. P53 and radiation responses. *Oncogene.* 2003;22:5774-5783.

28. Igea A, Nebreda AR. The Stress Kinase p38alpha as a Target for Cancer Therapy. *Cancer Res.* 2015;75:3997-4002.

29. Deak M, Clifton AD, Lucocq LM, Alessi DR. Mitogen- and stress-activated protein kinase-1 (MSK1) is directly activated by MAPK and SAPK2/p38, and may mediate activation of CREB. *EMBO J.* 1998;17:4426-4441.

30. Wagner EF, Nebreda AR. Signal integration by JNK and p38 MAPK pathways in cancer development. *Nat Rev Cancer.* 2009;9:537-549.

31. Kim MJ, Byun JY, Yun CH, Park IC, Lee KH, Lee SJ. c-Src-p38 mitogen-activated protein kinase signaling is required for Akt activation in response to ionizing radiation. *Mol Cancer Res.* 2008;6:1872-1880.

32. Marks PA, Breslow R. Dimethyl sulfoxide to vorinostat: development of this histone deacetylase inhibitor as an anticancer drug. *Nat Biotechnol.* 2007;25:84-90.

33. Li M, Liu D, Lee D, et al. Enhancing the Efficacy of Melanocortin 1 Receptor-Targeted Radiotherapy by Pharmacologically Upregulating the Receptor in Metastatic Melanoma. *Mol Pharm.* 2019;16:3904-3915.

34. Groselj B, Ruan JL, Scott H, et al. Radiosensitization In Vivo by Histone Deacetylase Inhibition with No Increase in Early Normal Tissue Radiation Toxicity. *Mol Cancer Ther.* 2018;17:381-392.

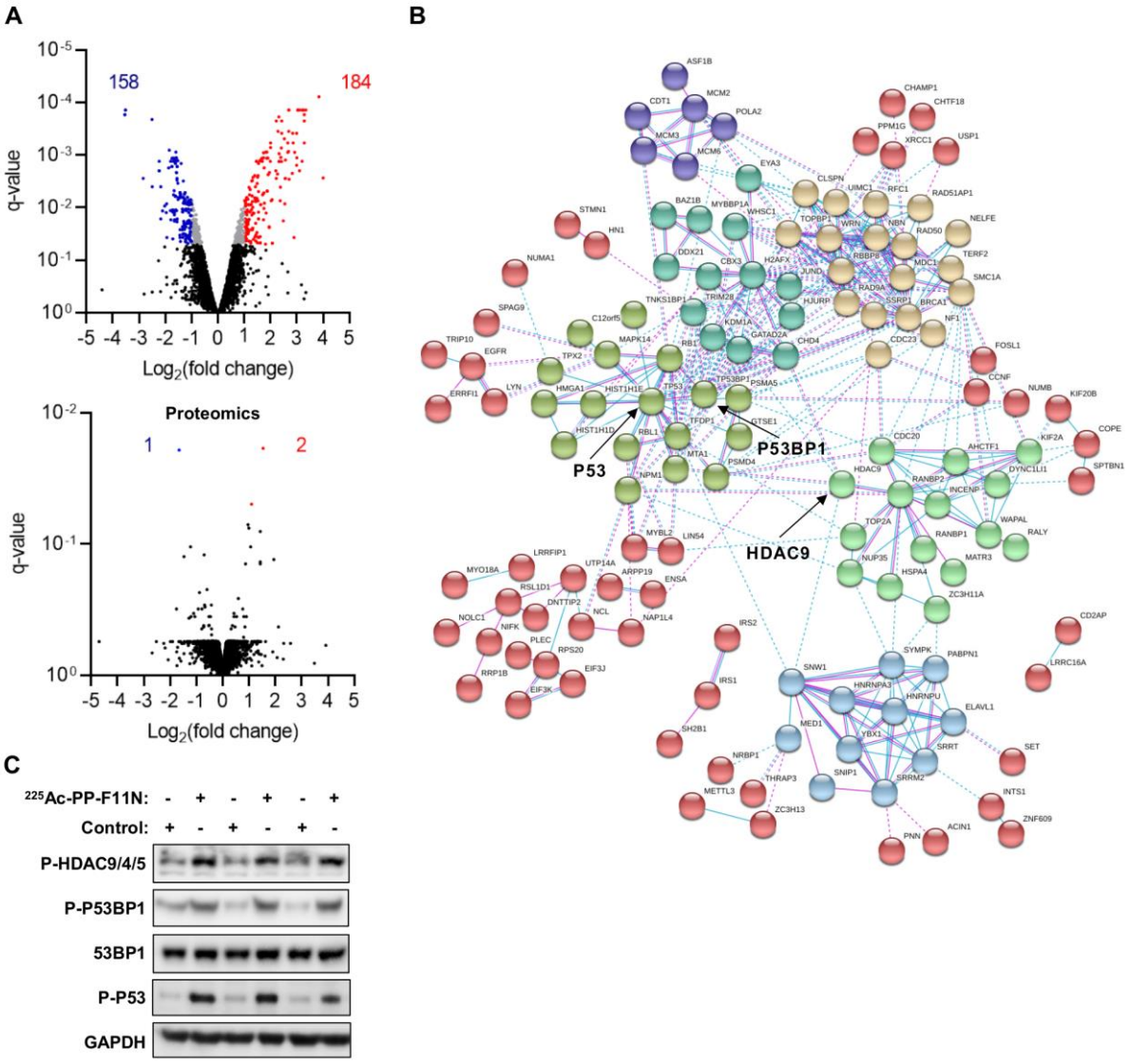

FIGURE 1. Cellular responses to targeted alpha-particle therapy with ^{225}Ac-PP-F11N.

(A) A431/CCKBR cells were treated with [^{255}Ac]Ac-PP-F11N and the generated tryptic peptides and phosphopeptide-enriched samples were subjected to proteomics and phosphoproteomics analysis, respectively. Volcano plots display phosphopeptide (phosphoproteomics) and protein (proteomics) abundance shown as log2 transformed fold change (FC). Red and blue dots indicate the significantly altered abundance of phosphopeptides or proteins. Q-value<0.05. (B) Interaction networks of proteins with altered phosphorylation or expression in response to ^{225}Ac-PP-F11N treatment. (C) WB analysis for the phosphorylation of HDAC9/4/5 at S246/S259/S220,

respectively; P53BP1 at S1778, P53 at S15, and for total P53BP1 and GAPDH in the protein lysates isolated from ^{225}Ac-PP-F11N-treated and untreated (control) cells.

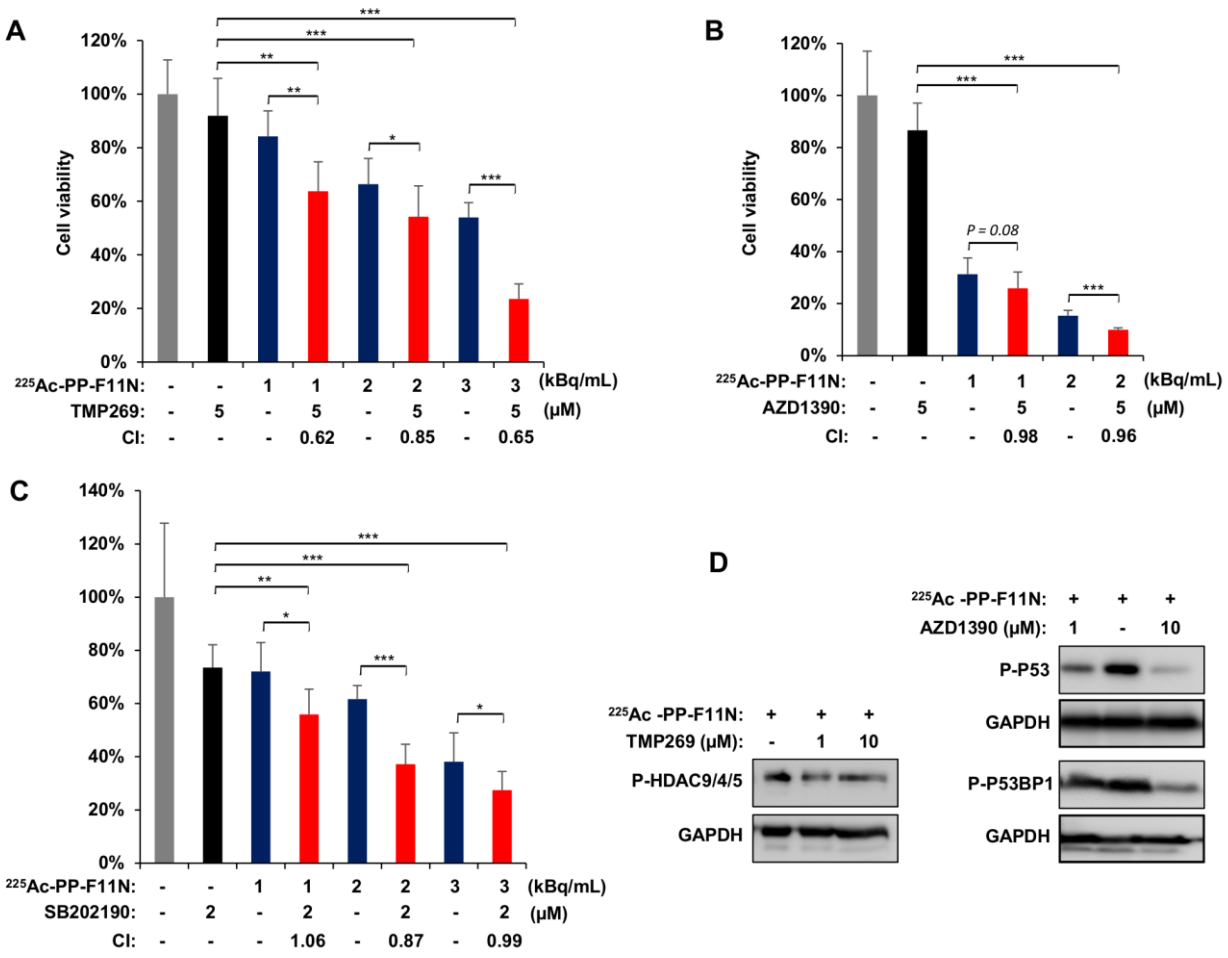

Figure 2. Treatment with HDAC, p38, and ATM inhibitors sensitizes A431/CCKBR cells to ^{225}Ac-PP-F11N.

Cell viability 48 h after treatment with ^{225}Ac-PP-F11N alone or in combination with HDACi TMP269 (A), ATMi AZD1390 (B), and p38i SB202190 (C). Bars represent mean ± SD. Corresponding combination index (CI) values between 0.9 and 1.1 indicate additive effects and below 0.9 synergism. (D) WB analysis for the phosphorylation of HDAC9/4/5 at S246/S259/S220, P53 at S15 as well as P53BP1 at S1778 in the protein lysates isolated from treated and control cells. Western blots were re-probed with antibody against GAPDH. *$p < 0.05$, **$p < 0.01$, ***$p < 0.001$.

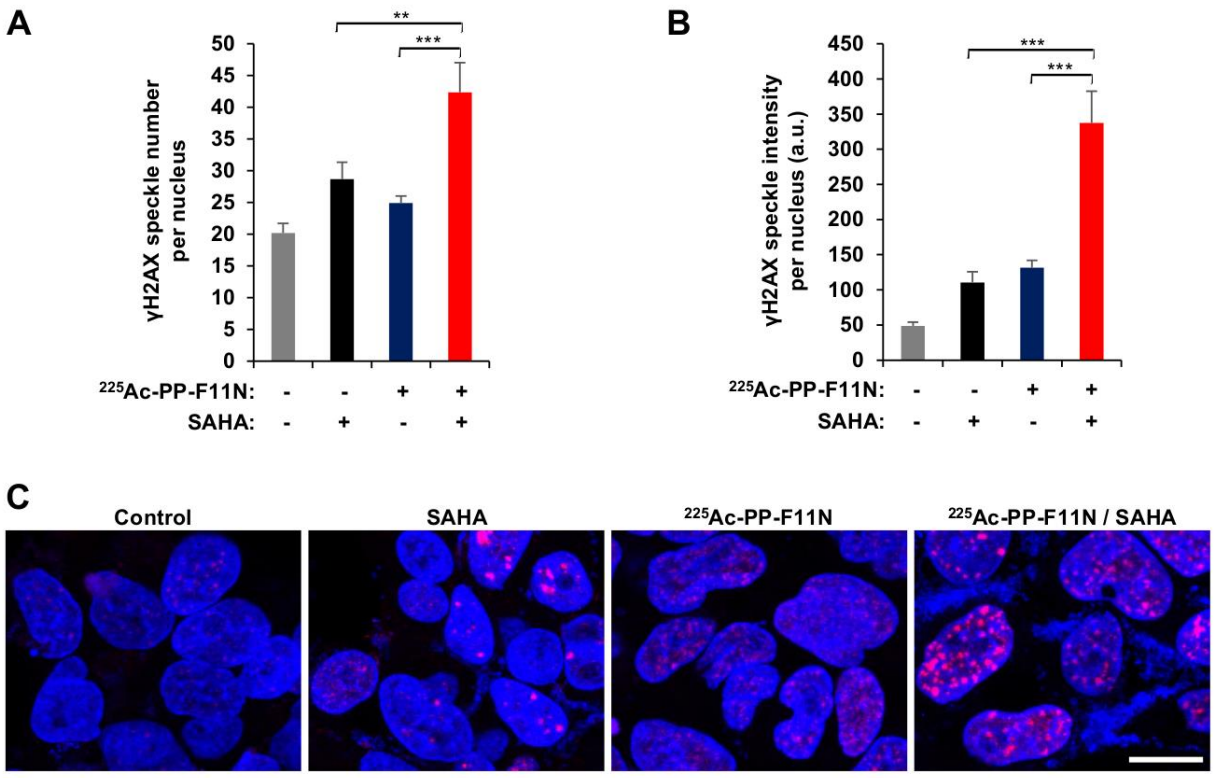

Figure 3. HDAC inhibition by SAHA increased the level of γH2AX in ^{225}Ac-PP-F11N-treated cells. A431/CCKBR cells were treated with 3 kBq/ml ^{225}Ac-PP-F11N or 2 μM SAHA alone or in combination for 24 h. (A, B) Bars represent means ± SEM of the numbers and intensities of γH2AX positive speckles per nucleus. (C) Typical images of treated and control cells. Red: γH2AX; Blue: Hoechst 33258. Scale bar: 20 μm. Arbitrary unit (a.u.). $^{**}p < 0.01$, $^{***}p < 0.001$.

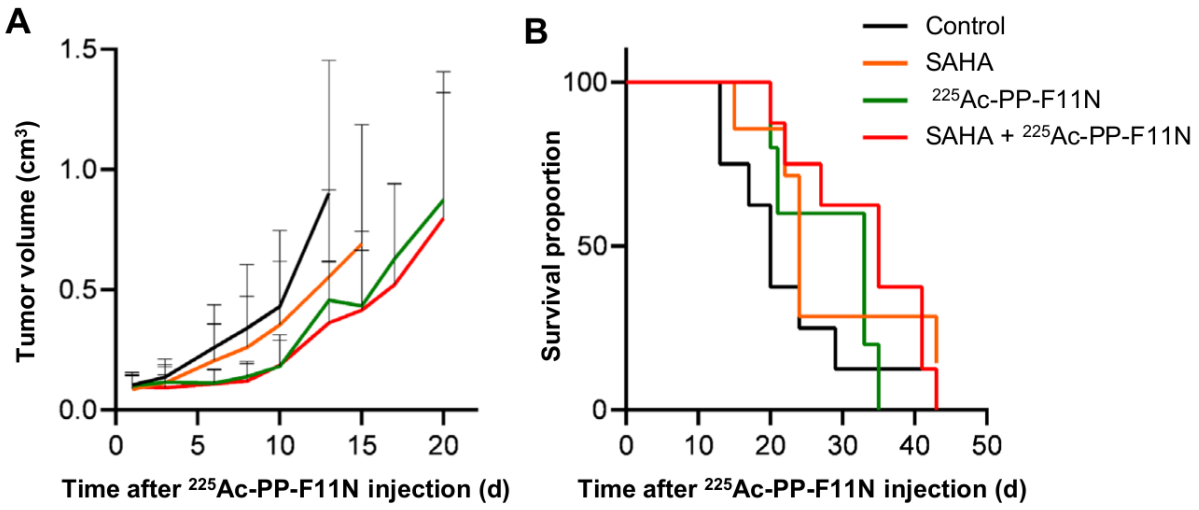

C

Treatments	Tumor volume (cm^3)	Survival (d)
Control	0.90 ± 0.55	22
^{225}Ac-PP-F11N	0.46 ± 0.16*	28
SAHA	0.55 ± 0.36	25
SAHA + ^{225}Ac-PP-F11N	0.36 ± 0.25*	33*

Figure 4. Tumor growth inhibition and prolonged survival in SAHA and ^{225}Ac-PP-F11N-treated mice.

(A) Tumor growth curves in A431/CCKBR xenografted mice after administration of ^{225}Ac-PP-F11N or PBS (control) alone or in combination with SAHA. Values represent mean ± SD. (B) The survival proportion presented as Kaplan-Meier curves of the control and different treatment groups. (C) Mean tumor volume ± SD on day 13 and survival in the control and different treatment groups. *$p < 0.05$.

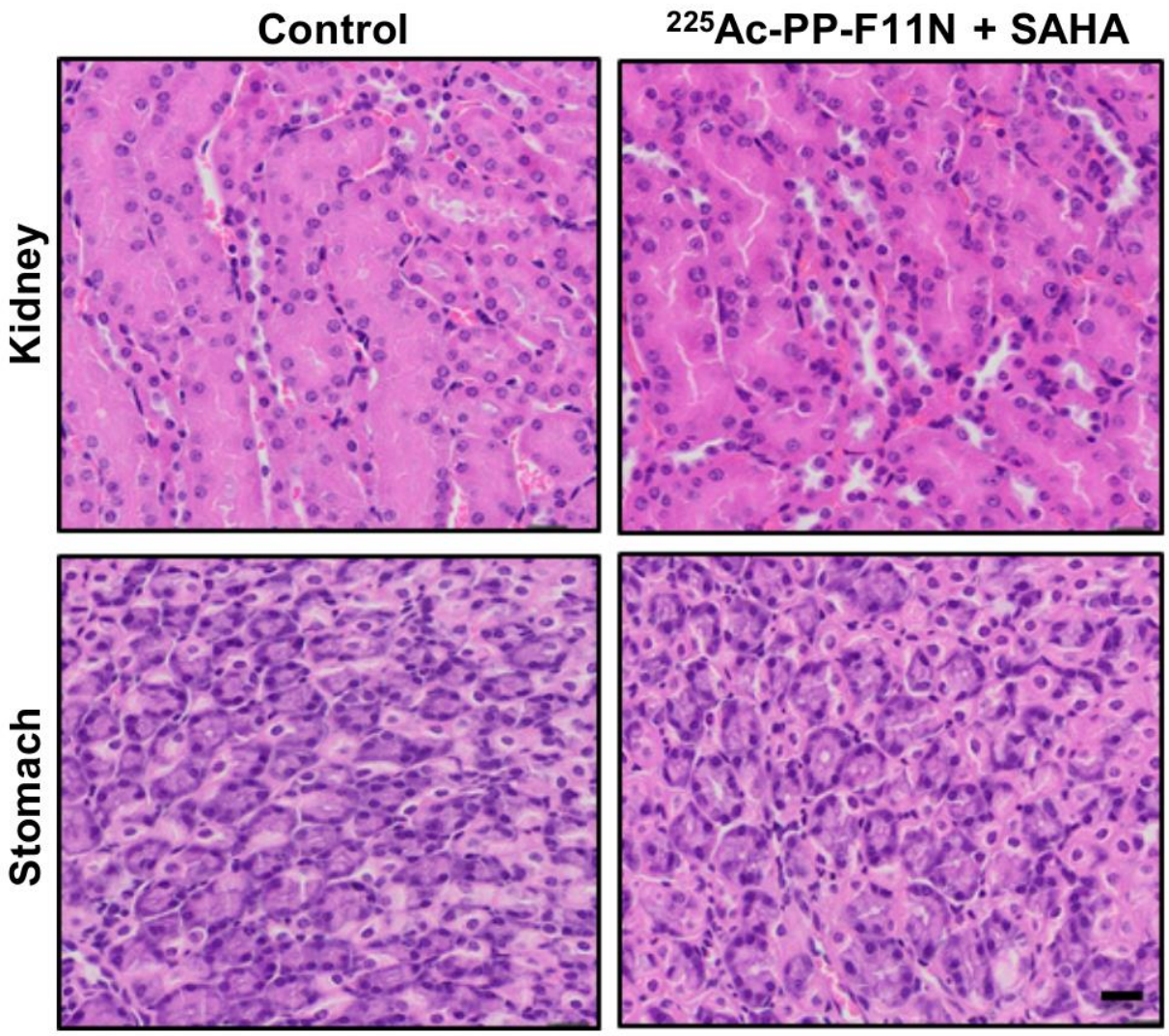

Figure 5. Histology of the kidney and stomach.

Representative images of the tissue sections stained with HE of the kidney and stomach isolated from control and ^{225}Ac-PP-F11N and SAHA-treated mice 35-43 days after injection of the activity. Scale bar: 20 μm

^{225}Ac-PP-F11N	Fold En.	*P-value*
DNA damage response, repair and nucleus structure		
DNA replication (BRCA1, POLA2, RAD50, RAD9A,RBBP8, SET, TICRR, WRN, CDT1, CHTF18, CLSPN, MCM2, MCM3AP, MCM3, MCM6, NBN, RFC1, SSRP1, TOPBP1) GOTERM_BP	9.1	3.1E-12
DNA repair (BRCA1, RAD50, RAD51AP1, RAD9A, RBBP8, TICRR, WRN, BOD1L1, CLSPN, NBN, NPM1, SMC1A, SSRP1, TOPBP1, TRIM28) GOTERM_BP	4.7	3.8E-6
Double-strand break repair via nonhomologous end joining (BRCA1, H2AFX, RAD50, WHSC1, MDC1, NBN, TP53BP1, UIMC1) GOTERM_BP	9.4	2.1E-5
Double-strand break repair via homologous recombination (BRCA1, H2AFX, RAD50, RAD51AP1, RBBP8, XRCC1, NBN, NUCKS1) GOTERM_BP	8.0	6.1E-5
Strand displacement (BRCA1, RAD50, RAD51AP1, RBBP8, WRN, NBN) GOTERM_BP	17.1	2.2E-5
DNA damage checkpoint (H2AFX, RAD9A, CLSPN, MAPK14, NBN, TP53BP1) GOTERM_BP	14.8	4.6E-5
DNA synthesis involved in DNA repair (BRCA1, RAD50, RAD51AP1, RBBP8, WRN, NBN) GOTERM_BP	12.7	9.9E-5
DNA unwinding involved in DNA replication (HMGA1, MCM2, MCM6, TOP2A) GOTERM_BP	29.6	2.7E-4
DNA double-strand break processing (BRCA1, RAD50, RBBP8, NBN) GOTERM_BP	19.7	9.7E-4
DNA duplex unwinding (RAD50, WRN, CHD4, MCM3, NBN) GOTERM_BP	8.4	2.8E-3
Nucleosome assembly (H2AFX, SET, ASF1B, HIST1H1D, HIST1H1E, MCM2, NPM1, NAP1L4) GOTERM_BP	5.0	1.1E-3
Telomere maintenance via telomerase (RAD50, RFC1, TNKS1BP1, TERF2) GOTERM_BP	16.4	1.7E-3
Covalent chromatin modification (RB1, RBL1, ASF1B, CBX3, C17orf49, TRIM28, ZMYND11) GOTERM_BP	4.6	4.3E-3
Telomere maintenance via recombination (POLA2, RAD50, WRN, RFC1) GOTERM_BP	9.2	9.0E-3
Cell cycle regulation		
Cell division (CD2AP, RBBP8, RB1, TPX2, TRIOBP, WAPL, ARPP19, CDC20, CDC23, CDCA2, CCNF, DYNC1LI1, ENSA, HELLS, KIF20B, KIF2A, MAP4, MISP, NUMA1, PSRC1, PKN2, SMC1A, ZC3HC1) GOTERM_BP	4.9	2.2E-9
Mitotic nuclear division (CD2AP, RBBP8, TPX2, TRIOBP, ARPP19, CDC20, CDC23, CDCA2, CCNF, DYNC1LI1, ENSA, HELLS, INCENP, KIF20B) GOTERM_BP	5.4	4.5E-8

Meiotic cell cycle (H2AFX, RBBP8, RBM7, NBN, NUMA1, ZNF318) GOTERM_BP	13.1	8.6E-5
Cell cycle (BRCA1, HJURP, RBL1, CDC20, CHTF18, LIN54, MCM2, NOLC1, PKN2, TERF2, TP53, ZMYND11) GOTERM_BP	4.1	1.8E-4
G1/S transition of mitotic cell cycle (POLA2, RANBP1, RBBPB8, RB1, CDT1, MCM2, MCM3, MCM6) GOTERM_BP	5.8	4.6E-4
Regulation of cell cycle (JUND, MYBL2, RB1, RBL1, CCNF, FIGNL1, LIN54, MED1) GOTERM_BP	4.8	1.4E-3
G2 DNA damage checkpoint (BRCA1, RBBP8, CLSPN, UIMC1) GOTERM_BP	14.8	2.3E-3
Cell cycle checkpoint (RBBP8, RB1, TICRR) GOTERM_BP	24.7	6.1E-3
Mitotic cell cycle checkpoint (RB1, TTK, NBN, SMC1A) GOTERM_BP	9.2	9.0E-3
Mitotic spindle organization (TTK, KIF2A, MAP4, STMN1, SMC1A) GOTERM_BP	12.3	6.7E-4
Chromosome segregation (BRCA1, HJURP, CDCA2, INCENP, PPP1R7, TOP2A) GOTERM_BP	6.5	2.2E-3
Sister chromatid cohesion (AHCTF1, RANBP2, WAPL, CDC20, INCENP, KIF2A, SMC1A) GOTERM_BP	5.0	2.7E-3
Signal transduction and cellular response		
Regulation of signal transduction by p53 class mediator (BRCA1, RAD50, RAD9A, RBBP8, TPX2, WRN, CHD4, MAPK14, NBN, SSRP1, TOPBP1, TP53) GOTERM_BP	7.2	9.2E-7
Cellular response to DNA damage stimulus (BRCA1, H2AFX, LYN, RAD50, RAD9A, TIGAR, WRN, BOD1L1, BAZ1B, TOP2A, TOPBP1, TP53BP1, TP53) GOTERM_BP	4.6	2.6E-5
Response to ionizing radiation (BRCA1, EYA3, H2AFX, TICRR, MTA1, TOPBP1, UIMC1) GOTERM_BP	10.6	4.8E-5
Cellular response to ionizing radiation (RAD51AP1, RAD9A, FIGNL1, MAPK14, TP53) GOTERM_BP	11.9	7.6E-4
Cellular response to epidermal growth factor stimulus (ERRFI1, ZFP36L2, ZFP36, EGFR, MED1) GOTERM_BP	11.2	9.6E-4
Cellular response to dexamethasone stimulus (ERRFI1, CBX3, EGFR, HNRNPU) GOTERM_BP	10.2	6.8E-3
DNA damage response, signal transduction by p53 class mediator resulting in cell cycle arrest (GTSE1, NPM1, TNKS1BP1, TFDP1, TP53) GOTERM_BP	6.0	9.7E-3
ATM Signaling Pathway (BRCA1, RAD50, RBBP8, NBN, TP53) BIOCARTA	8.6	2.0E-3
Role of BRCA1, BRCA2 and ATR in Cancer Susceptibility (BRCA1, RAD50, RAD9A, NBN, TP53) BIOCARTA	8.2	2.4E-3

TABLE 1. Significantly enriched (P<0.01) biological processes and signal transduction pathways in response to ^{225}Ac-PP-F11N treatment.

Graphical Abstract

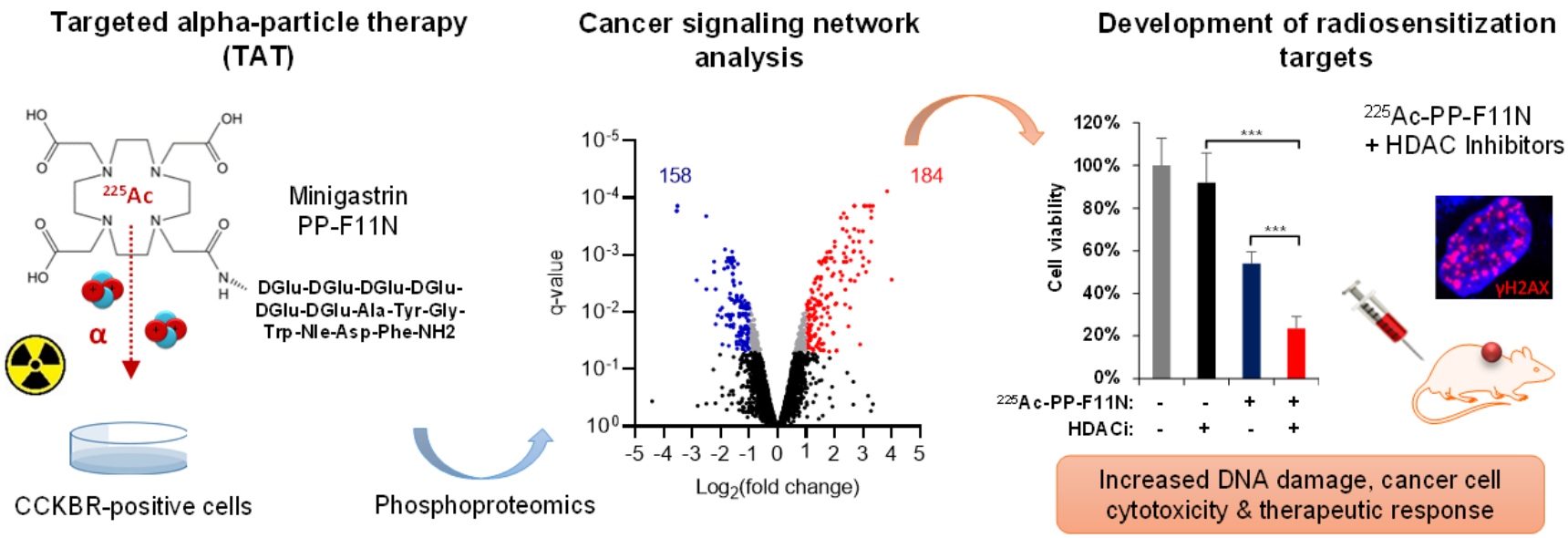

Supplemental Table 1. Significantly increased phosphopeptide abundance in A431/CCKBR cells treated with ^{225}Ac-PP-F11N. MS-based quantification: $\log_2$ ratio > |1| and q < 0.05.

LOG_2 (ratio) ^{225}Ac-PP-F11N / CON	*q*-VALUE	| UniProt |SYMBOL; NAME	SEQUENCE WINDOW POSITION (PROBABILITY>0.75)
4.00	0.00272	|Q14980|NUMA1; Nuclear mitotic apparatus protein 1	LSQLEEHLS(1)QLQDNPPQEK
3.84	7.75E-05	|Q8TAD8|SNIP1; Smad nuclear-interacting protein 1	NDVGGGGSES(1)QELVPR
3.34	0.00013	|P17096|HMGA1; High mobility group protein HMG-I/HMG-Y	KQPPVSPGTALVGS(1)QKEPSEVPTPK
3.28	0.00022	|Q9BVJ6|UT14A; U3 small nucleolar RNA-associated protein 14 homolog A	DSGS(1)QEVLSELR
3.28	0.00017	|Q14676|MDC1; Mediator of DNA damage checkpoint protein 1	QDGS(1)QEAPEAPLSSELEPFHPK
3.28	0.00058	|Q969E4|TCAL3; Transcription elongation factor A protein-like 3	GTDDSPKDS(1)QEDLQER
3.25	0.00013	|Q13428|TCOF; Treacle protein	GSLGS(1)QGAKDEPEEELQK
3.21	0.00013	|Q14566|MCM6; DNA replication licensing factor MCM6	MDLAAAAEPGAGS(1)QHLEVR
3.20	0.00131	|Q9H6F5|CCD86; Coiled-coil domain-containing protein 86	CS(1)QDQGVLASELAQNK
3.11	0.00013	|O60934|NBN; Nibrin	MLS(1)QDAPTVK
3.10	0.00199	|Q12888|TP53B; Tumor suppressor p53-binding protein 1	EEGGCSLASTPATTLHLLQLS(1)GQR
3.04	0.00013	|Q15435|PP1R7; Protein phosphatase 1 regulatory subunit 7	GAGQQQS(1)QEMMEVDR
3.03	0.00013	|Q16539|MK14; Mitogen-activated protein kinase 14	S(1)QERPTFYR
3.00	0.00112	|Q13451|FKBP5; Peptidyl-prolyl cis-trans isomerase FKBP5	GTDS(1)QAMEEEKPEGHV
2.99	0.00038	|Q86U42|PABP2; Polyadenylate-binding protein 2	APPGAPGPGPGSGAPGS(1)QEEEEEPGLVEGDPG DGAIEDPELEAIK
2.99	0.00156	|O43768|ENSA; Alpha-endosulfine	S(1)QKQEEENPAEETGEEK
2.91	0.00089	|O95232|LC7L3; Luc7-like protein 3	IDVLLQQIEELGS(1)EGKVEEAQGMMK
2.89	0.03692	|P51522|ZNF83; Zinc finger protein 83	S(1)NLASHQRIHTGEK
2.86	0.00058	|Q86U44|MTA70; N6-adenosine-methyltransferase 70 kDa subunit	DHTPS(1)QELALTQSVGGDSSADR
2.84	0.00038	|P25205|MCM3; DNA replication licensing factor MCM3	APGEQDGDAMPLGSAVDILATDDPNFS(1)QEDQ QDTQIYEK
2.83	0.00222	|O94782|UBP1; Ubiquitin carboxyl-terminal hydrolase 1	ALDFTDS(1)QENEEK
2.70	0.00289	|Q12888|TP53B; Tumor suppressor p53-binding protein 1	LVSPETEAS(1)EES(1)LQFNLEKPATGER
2.70	0.00013	|Q7Z5K2|WAPL; Wings apart-like protein homolog	SEDCILSLDS(1)DPLLEMK
2.69	0.00035	|P68402|PA1B2; Platelet-activating factor acetylhydrolase IB subunit beta	S(1)QGDSNPAAIPHAAEDIQGDDR
2.69	0.00013	|Q99733|NP1L4; Nucleosome assembly protein 1-like 4	ADHSFS(0.99)DGVPS(1)DSVEAAK
2.68	0.00085	|Q92547|TOPB1; DNA topoisomerase 2-binding protein 1	NAVALSAS(0.99)PQLK
2.66	0.00058	|Q13573|SNW1; SNW domain-containing protein 1	ALTSFLPAPTQLS(1)QDQLEAEEK
2.65	0.00089	|Q14683|SMC1A; Structural maintenance of chromosomes protein 1A	GTMDDISQEEGSS(0.99)QGEDSVSGSQR
2.56	0.00123	|Q96RL1|UIMC1; BRCA1-A complex subunit RAP80	EVNS(1)QEEEEEELLR
2.56	0.00277	|Q12888|TP53B; Tumor suppressor p53-binding protein 1	LVSPETEAS(1)EES(1)LQFNLEKPATGER
2.56	0.00277	|Q12888|TP53B; Tumor suppressor p53-binding protein 1	LVSPETEAS(1)EES(1)LQFNLEKPATGER
2.54	0.00841	|Q9Y696|CLIC4; Chloride intracellular channel protein 4	LDEYLNSPLPDEIDENS(1)MEDIK
2.52	0.00049	|Q9BVJ6|UT14A; U3 small nucleolar RNA-associated protein 14 homolog A	SELSQDAEPAGS(1)QETK
2.48	0.01792	|Q7RTP6|MICA3; Protein-methionine sulfoxide oxidase MICAL3	GPSQATSPIRS(0.91)PQESALLFIPVHSPSTEGPQL PPVPAATQEK

2.43	0.00022	|Q14566|MCM6; DNA replication licensing factor MCM6	EIESEIDS(1)EEELINK
2.42	0.00038	|Q92878|RAD50; DNA repair protein RAD50	LFDVCGS(1)QDFESDLDR
2.42	0.00132	|Q9H1E3|NUCKS; Nuclear ubiquitous casein and cyclin-dependent kinase substrate 1	SGKNS(1)QEDSEDSEDKDVK
2.40	0.00073	|P20810|ICALM Calpastatin	SESELIDELS(1)EDFDR
2.39	0.00111	|Q96B01|R51A1; RAD51-associated protein 1	ELPTVTTNVQNS(1)QDK
2.38	0.00406	|O00192|ARVC; Armadillo repeat protein deleted in velo-cardio-facial syndrome	GALS(1)PGGFDDSTLPLVDK
2.37	0.00736	|O60934|NBN; Nibrin	MDIETNDTFSDEAVPESSKIS(0.99)QENEIGK
2.33	0.00094	|P16104|H2AX; Histone H2AX	ATQAS(1)QEY
2.33	0.00132	|Q9NZT2|OGFR; Opioid growth factor receptor	S(1)QGDEAGGHGEDRPEPLS(1)PK
2.33	0.00132	|Q9NZT2|OGFR; Opioid growth factor receptor	S(1)QGDEAGGHGEDRPEPLS(1)PK
2.32	0.00018	|Q13185|CBX3; Chromobox protein homolog 3	LTWHS(0.99)CPEDEAQ
2.29	0.00035	|Q14839|CHD4; Chromodomain-helicase-DNA-binding protein 4	QVNYNDGS(1)QEDR
2.27	0.0023	|Q15554|TERF2; Telomeric repeat-binding factor 2	LVLEEDSQSTEPSAGLNSS(0.83)QEAASAPPSKPTVLNQPLPGEK
2.22	0.00277	|Q13263|TIF1B; Transcription intermediary factor 1-beta	QGSGSS(0.93)QPMEVQEGYGFGSGDDPYSSAEPHVSGVK
2.22	0.00022	|Q9UQ35|SRRM2; Serine/arginine repetitive matrix protein 2	EQNSALPTSS(0.99)QDEELMEVVEK
2.20	0.00199	|Q15326|ZMY11; Zinc finger MYND domain-containing protein 11	KEEPEPETEAVSSS(0.94)QEIPTMPQPIEK
2.06	0.04741	|Q9NXH9|TRM1; tRNA (guanine(26)-N(2))-dimethyltransferase	SALLHADFRVS(1)LS(1)HACK
2.06	0.04741	|Q9NXH9|TRM1; tRNA (guanine(26)-N(2))-dimethyltransferase	SALLHADFRVS(1)LS(1)HACK
2.06	0.00707	|Q99575|POP1; Ribonucleases P/MRP protein subunit POP1	SAVCIADPLPTPS(1)QEK
2.03	0.00736	|Q14839|CHD4; Chromodomain-helicase-DNA-binding protein 4	IEENS(1)LKEEESIEGEK
2.00	0.00058	|Q6PIW4|FIGL1; Fidgetin-like protein 1	FSVCGSS(0.95)QESDSLPNSAHDR
2.00	0.00071	|Q8IZ73|RUSD2; RNA pseudouridylate synthase domain-containing protein 2	QSLDVLDLCEGDLS(1)PGLTDSTAPSSELGKDDLEELAAAAQK
1.99	0.00131	|Q96G28|CFA36; Cilia- and flagella-associated protein 36	TEEPTVHSSEAAIMNNS(1)QGDGEHFAHPPSEVK
1.95	0.00214	|Q96RL1|UIMC1; BRCA1-A complex subunit RAP80	SRPLATGPSS(0.94)QSHQEK
1.95	0.02386	|P20810|ICAL; Calpastatin	EQLPPMSEDFLLDALS(0.99)EDFSGPQNASSLK
1.95	0.02325	|Q9HB58|SP110; Sp110 nuclear body protein	MNAEEDS(1)EEMPSLLTSTVQVASDNLIPQIR
1.91	0.00235	|Q9H307|PININ; Pinin	QQDS(1)QPEEVMDVLEMVENVK
1.90	0.00113	|P38398|BRCA1; Breast cancer type 1 susceptibility protein	VVDVEEQQLEES(1)GPHDLTETSYLPR
1.87	0.00485	|Q12888|TP53B; Tumor suppressor p53-binding protein 1	QSQQPMKPIS(1)PVKDPVSPASQK
1.87	0.00485	|Q12888|TP53B; Tumor suppressor p53-binding protein 1	QSQQPMKPIS(1)PVKDPVS(1)PAS(1)QK
1.87	0.00485	|Q12888|TP53B; Tumor suppressor p53-binding protein 1	QSQQPMKPIS(1)PVKDPVS(1)PAS(1)QK
1.86	0.00115	|P10155|RO60; 60 kDa SS-A/Ro ribonucleoprotein	QIANS(1)QDGYVWQVTDMNR
1.86	0.00087	|P43243|MATR3; Matrin-3	S(1)QESGYYDR
1.83	0.01266	|O75607|NPM3; Nucleoplasmin-3	AAGTAAALAFLS(0.97)QESR
1.82	0.00087	|P18615|NELFE; Negative elongation factor E	SLS(1)EQPVMDTATATEQAK
1.81	0.04942	|P49736|MCM2; DNA replication licensing factor MCM2	AIPELDAYEAEGLALDDEDVEELTAS(0.99)QR
1.77	0.00821	|Q9UQ35|SRRM2; Serine/arginine repetitive matrix protein 2	HGGSPQPLATTPLS(0.99)QEPVNPPSEAS(0.82)PTR
1.76	0.00175	|Q9BWU0|NADAP; Kanadaptin	ETQTHENMSQLS(1)EEEQNK
1.75	0.01034	|O43719|HTSF1; HIV Tat-specific factor 1	GFEGSCS(1)QKESEEGNPVR
1.74	0.00526	|P78332|RBM6; RNA-binding protein 6	EGETQGVAFEHESPADFQNS(1)QS(1)PVQDQDK
1.74	0.00526	|P78332|RBM6; RNA-binding protein 6	EGETQGVAFEHESPADFQNS(1)QS(1)PVQDQDK

1.73	0.00113	|P26651|TTP; mRNA decay activator protein ZFP36	LGPELSPSPTS(0.92)PTATSTTPSR
1.73	0.01695	|Q12888|TP53B; Tumor suppressor p53-binding protein 1	LPDGPTGS(0.98)S(0.99)EEEEEFLEIPPFNK
1.73	0.00090	|P19338|NUCL; Nucleolin	GFGFVDFNS(1)EEDAK
1.70	0.00570	|Q9Y580|RBM7; RNA-binding protein 7	SFS(1)SPENFQR
1.69	0.00131	|Q9C0C2|TB182; 182 kDa tankyrase-1-binding protein	GSGGLFS(1)PSTAHVPDGALGQR
1.69	0.00131	|Q9C0C2|TB182; 182 kDa tankyrase-1-binding protein	GS(1)GGLFS(0.96)PSTAHVPDGALGQR
1.66	0.00114	|Q13263|TIF1B; Transcription intermediary factor 1-beta	S(1)GEGEVSGLMR
1.62	0.00877	|P49757|NUMB; Protein numb homolog	IVVGSSVAPGNTAPSPSS(0.99)PTS(0.99)PTSDAT TSLEMNNPHAIPR
1.62	0.00877	|P49757|NUMB; Protein numb homolog	IVVGSSVAPGNTAPSPSS(0.99)PTS(0.99)PTSDAT TSLEMNNPHAIPR
1.61	0.04667	|P04637|P53; Cellular tumor antigen p53	MEEPQS(1)DPSVEPPLS(0.99)QETFSDLWK
1.61	0.00128	|Q96RL1|UIMC1; BRCA1-A complex subunit RAP80	LLLEEEPTTSHGQSS(0.88)QGIVEETSEEGNSVPAS QSVAALTSK
1.61	0.03573	|Q9H2P0|ADNP; Activity-dependent neuroprotector homeobox protein	KLDDDSDS(0.99)PSFFEEKPEEPVVLALDPK
1.61	0.04715	|Q8N201|INT1; Integrator complex subunit 1	EGEEVYS(1)WSESQDQVFLR
1.60	0.00128	|Q9NYF8|BCLF1; Bcl-2-associated transcription factor 1	S(1)QEEPKDTFEHDPSESIDEFNK
1.54	0.00495	|P04637|P53; Cellular tumor antigen p53	MEEPQS(1)DPSVEPPLS(0.99)QETFSDLWK
1.54	0.01212	|Q99708|COM1; DNA endonuclease RBBP8	CS(1)PDNKPSLQIK
1.54	0.01631	|Q9NRF2|SH2B1; SH2B adapter protein 1	ASGSLSPPILAPLS(1)PGAEISPHDLSLESCR
1.54	0.01631	|Q9NRF2|SH2B1; SH2B adapter protein 1	ASGSLS(0.94)PPILAPLS(1)PGAEISPHDLSLESCR
1.54	0.00144	|Q9UK76|HN1; haematological and neurological expressed 1 protein	GEGDIHENVDTDLPGS(1)LGQSEEKPVPAAPVPSP VAPAPVPSR
1.54	0.03680	|O00139|KIF2A; Kinesin-like protein KIF2A	EIDLESIFSLNPDLVPDEEIEPS(1)PET(0.99)PPPPAS SAK
1.54	0.03680	|O00139|KIF2A; Kinesin-like protein KIF2A	EIDLESIFSLNPDLVPDEEIEPS(1)PET(0.99)PPPPAS SAK
1.53	0.00246	|Q01105|SET; Protein SET	LNEQAS(1)EEILK
1.52	0.00736	|Q969E4|TCAL3; Transcription elongation factor A protein-like 3	REDEGEPGDEGQLEDEGS(1)QEK
1.50	0.00263	|O60784|TOM1; Target of Myb protein 1	GLEFPMTDLDMLS(1)PIHT(1)PQR
1.50	0.04679	|P85037|FOXK1; Forkhead box protein K1	EEAPAS(1)PLRPLYPQIS(1)PLK
1.49	0.00348	|Q9BQG0|MBB1A; Myb-binding protein 1A	SPS(1)LLQSGAK
1.48	0.02957	|O15355|PPM1G; Protein phosphatase 1G	KLEEVLS(0.91)TEGAEENGNSDK
1.48	0.00662	|P47974|TISD; Zinc finger protein 36, C3H1 type-like 2	RHS(0.99)ASNLHALAHPAPSPGSCSPK
1.46	0.00131	|Q12888|TP53B; Tumor suppressor p53-binding protein 1	HEEQS(1)NEDIPIAEQSSK
1.46	0.00131	|Q12888|TP53B; Tumor suppressor p53-binding protein 1	QDKPMDTSVLS(1)EEGGEPFQK
1.44	0.00765	|P49366|DHYS; Deoxyhypusine synthase	KLEPLS(1)QDEDQHADLTQSR
1.44	0.00662	|Q9C0C2|TB182; 182 kDa tankyrase-1-binding protein	GSGGLFS(1)PSTAHVPDGALGQR
1.44	0.04306	|Q13501|SQSTM; Sequestosome-1	SSS(0.92)QPSSCCSDPSKPGGNVEGATQSLAEQM R
1.44	0.033	|Q07157|ZO1; Tight junction protein ZO-1	PVYAQVGQPDVDLPVS(1)PSDGVLPNSTHEDGILR
1.43	0.01988	|Q99611|SPS2; Selenide, water dikinase 2	GLVGGQEEAS(1)QEAGLPAGAGPSPTFPALGIGM DSCVIPLR
1.42	0.00715	|Q8ND82|Z280C; Zinc finger protein 280C	GTNTSS(0.85)PYDAGADYLR
1.42	0.00398	|O75822|EIF3J; Eukaryotic translation initiation factor 3 subunit J	VLT(1)PEEQLADK
1.41	0.03582	|Q8IVT2|MISP; Mitotic interactor and substrate of PLK1	NALFPEVFS(0.97)PTPDENSDQNSR
1.40	0.00655	|Q12888|TP53B; Tumor suppressor p53-binding protein 1	LS(1)DVDANTAIK
1.40	0.00246	|Q9UQ35|SRRM2; Serine/arginine repetitive matrix protein 2	ENS(1)FGS(1)PLEFR

1.37	0.01278	|Q12888|TP53B; Tumor suppressor p53-binding protein 1	TSS(1)GTSLSAMHSSGSSGK
1.35	0.03983	|Q00839|HNRPU; Heterogeneous nuclear ribonucleoprotein U	PAMEPGNGS(1)LDLGGDSAGR
1.34	0.01269	|Q9Y6W5|WASF2; Wiskott-Aldrich syndrome protein family member 2	SSVVS(0.97)PSHPPPAPPLGSPPGPK
1.34	0.00263	|Q12888|TP53B; Tumor suppressor p53-binding protein 1	GNLLHFPSS(1)QGEEEKEK
1.33	0.00983	|Q9HAW4|CLSPN; Claspin	SLS(0.99)SDSTLLLFK
1.32	0.02456	|Q9BYG3|MK67I; MKI67 FHA domain-interacting nucleolar phosphoprotein	S(1)QVAELNDDDKDDEIVFK
1.31	0.00306	|P15407|FOSL1; Fos-related antigen 1	SSSSSGDPSSDPLGS(1)PTLLAL
1.31	0.00765	|Q9UBQ5|EIF3K; Eukaryotic translation initiation factor 3 subunit K	IDFDSVSSIMASS(0.99)Q
1.30	0.02611	|A1L390|PKHG3; Pleckstrin homology domain-containing family G member 3	KPVLSLFDYEQLMAQEHS(1)PPKPSSAGEMSPQR
1.30	0.02611	|A1L390|PKHG3; Pleckstrin homology domain-containing family G member 3	KPVLSLFDYEQLMAQEHS(0.99)PPKPSSAGEMS(0.81)PQR
1.30	0.00597	|Q9Y4H2|IRS2; Insulin receptor substrate 2	HNS(1)ASVENVSLR
1.29	0.01374	|P28066|PSA5; Proteasome subunit alpha type-5	ITS(1)PLMEPSSIEK
1.28	0.00311	|P27816|MAP4; Microtubule-associated protein 4	S(0.99)PSTLLPK
1.27	0.01093	|O14579|COPE; Coatomer subunit epsilon	APPAPGPASGGS(0.99)GEVDELFDVK
1.27	0.02613	|Q3KQU3|MA7D1; MAP7 domain-containing protein 1	PASPCPSPGPGHT(0.92)LPPKPPSPR
1.26	0.00869	|Q12888|TP53B; Tumor suppressor p53-binding protein 1	SGTAETEPVEQDSS(0.99)QPSLPLVR
1.25	0.04715	|P60866|RS20; 40S ribosomal protein S20	DTGKT(0.99)PVEPEVAIHR
1.24	0.04411	|P18615|NELFE; Negative elongation factor E	SDS(0.99)FPER
1.23	0.00878	|Q9Y6W5|WASF2; Wiskott-Aldrich syndrome protein family member 2	RSS(0.76)VVS(0.95)PSHPPPAPPLGSPPGPK
1.23	0.00452	|Q9C0C2|TB182; 182 kDa tankyrase-1-binding protein	NMAPGAVCS(1)PGESK
1.21	0.01208	|P34932|HSP74; Heat shock 70 kDa protein 4	MQVDQEEPHVEEQQQQTPAENKAES(0.99)EEMETSQAGSK
1.20	0.00570	|Q8NFH5|NUP53; Nucleoporin NUP53	CALSS(1)PSLAFTPPIK
1.19	0.01691	|P16402|H13; Histone H1.3	S(0.85)ETAPLAPTIPAPAEK
1.18	0.00410	|Q5VZK9|CARL1; F-actin-uncapping protein LRRC16A	S(1)PPVDCPR
1.18	0.01675	|Q15642|CIP4; Cdc42-interacting protein 4	NKPRPPPLS(1)PLGGPVPSALPNGPPS(1)PR
1.18	0.01675	|Q15642|CIP4; Cdc42-interacting protein 4	NKPRPPPLS(1)PLGGPVPSALPNGPPS(1)PR
1.17	0.04306	|P35611|ADDA; Alpha-adducin	AAVVTS(1)PPPTTAPHK
1.16	0.00877	|P17096|HMGA1; High mobility group protein HMG-I/HMG-Y	EPSEVPT(1)PK
1.16	0.00877	|P17096|HMGA1; High mobility group protein HMG-I/HMG-Y	KQPPVSPGTALVGS(1)QKEPSEVPTPK
1.16	0.02860	|Q9UKV3|ACINU; Apoptotic chromatin condensation inducer in the nucleus	LSEGS(1)QPAEEEEDQETPSR
1.14	0.03153	|Q8IY33|MILK2; MICAL-like protein 2	PGRPLS(1)PANVPALPGETVTS(0.79)PVR
1.14	0.03153	|Q8IY33|MILK2; MICAL-like protein 2	PGRPLS(1)PANVPALPGETVTS(0.79)PVR
1.14	0.01888	|Q9UQ35|SRRM2; Serine/arginine repetitive matrix protein 2	SEEPAGQILSHLS(0.93)SELK
1.14	0.00693	|P43358|MAGA4; Melanoma-associated antigen 4	QPNEGSS(0.98)S(1)QEEEGPSTSPDAESLFR
1.14	0.02578	|Q8N1G2|CMTR1; Cap-specific mRNA (nucleoside-2-O-)-methyltransferase 1	QHSSDS(0.94)FDDAFK
1.14	0.02075	|P16949|STMN1; Stathmin	RAS(1)GQAFELILS(1)PR
1.13	0.02855	|Q9H7M9|VISTA; V-type immunoglobulin domain-containing suppressor of T-cell activation	HLLSEPSTPLS(0.82)PPGPGDVFFPSLDPVPDS(0.94)PNFEVI
1.12	0.01815	|Q9BXP5|SRRT; Serrate RNA effector molecule homolog	NITDYLIEEVSAEEEELLGSS(0.8)GGAPPEEPPK
1.12	0.01109	|Q9NX74|DUS2L; tRNA-dihydrouridine(20) synthase [NAD(P)+]-like	KPFVALGSGEES(1)PLEGW

1.10	0.02934	|Q09666|AHNK; Neuroblast differentiation-associated protein AHNAK	MYFPDVEFDIKS(1)PK
1.10	0.01208	|P47974|TISD; Zinc finger protein 36, C3H1 type-like 2	RHS(0.99)ASNLHALAHPAPSPGSCSPK
1.10	0.01372	|Q9UJM3|ERRFI; ERBB receptor feedback inhibitor 1	EPLS(1)PSNSR
1.09	0.00641	|Q9UKV0|HDAC9; Histone deacetylase 9	TQS(0.99)APLPQSTLAQLVIQQQHQQFLEK
1.09	0.00663	|Q8NC51|PAIRB; Plasminogen activator inhibitor 1 RNA-binding protein	DELTES(1)PK
1.09	0.03903	|Q9NYZ3|GTSE1; G2 and S phase-expressed protein 1	PSPVVGQLIDLSSPLIQLS(1)PEADKENVDSPLLK
1.09	0.01998	|Q9C0C2|TB182; 182 kDa tankyrase-1-binding protein	EEAGKEEPPPLT(1)PPAR
1.08	0.03001	|Q9H201|EPN3; Epsin-3	TPVLPAGPPTTDPWALNS(1)PHHK
1.08	0.02288	|Q13263|TIF1B; Transcription intermediary factor 1-beta	QGS(0.99)GSSQPMEVQEGYGFGSGDDPYSSAEP HVSGVK
1.07	0.02535	|O15014|ZN609; Zinc finger protein 609	APS(0.99)LTDLVK
1.06	0.01760	|Q7Z3T8|ZFY16; Zinc finger FYVE domain-containing protein 16	NEIIQS(0.99)PISQVPSVEK
1.06	0.02855	|Q08357|S20A2; Sodium-dependent phosphate transporter 2	VQEAES(1)PVFK
1.05	0.01813	|Q32MZ4|LRRF1; Leucine-rich repeat flightless-interacting protein 1	ALDS(1)NSLENDDLSAPGR
1.05	0.03443	|Q86WB0|NIPA; Nuclear-interacting partner of ALK	S(1)WDSSSPVDRPEPEAASPTTR
1.05	0.00825	|Q9UHY1|NRBP; Nuclear receptor-binding protein	PQQPQQEEVTS(0.99)PVVPPSVK
1.05	0.00736	|P17535|JUND; Transcription factor jun-D	LAS(1)PELER
1.05	0.04258	|Q5VUA4|ZN318; Zinc finger protein 318	YISQEEGPLS(1)PFLGQLDEDYR
1.05	0.04258	|Q5VUA4|ZN318; Zinc finger protein 318	YIS(1)QEEGPLS(1)PFLGQLDEDYR
1.05	0.01811	|Q13887|KLF5; Krueppel-like factor 5	QAEMLQNLT(1)PPPSYAATIASK
1.05	0.00932	|Q86W92|LIPB1; Liprin-beta-1	ALEYSNGIFDCQS(1)PTS(0.99)PFMGSLR
1.05	0.00932	|Q86W92|LIPB1; Liprin-beta-1	ALEYSNGIFDCQS(1)PTS(0.99)PFMGSLR
1.05	0.03692	|Q8NFC6|BD1L1; Biorientation of chromosomes in cell division protein 1-like 1	RLS(0.98)ESLHVVDENKNESK
1.05	0.00736	|Q96JY6|PDLI2; PDZ and LIM domain protein 2	AGS(1)PFS(1)PPPSSSSLTGEAAISR
1.04	0.02322	|Q9HCN4|GPN1; GPN-loop GTPase 1	DSLS(1)PVLHPSDLILTR
1.04	0.01810	|P67809|YBOX1; Nuclease-sensitive element-binding protein 1	S(1)VGDGETVEFDVVEGEK
1.04	0.01813	|P55036|PSMD4; 26S proteasome non-ATPase regulatory subunit 4	AAAASAAEAGIATTGTEDS(1)DDALLK
1.04	0.01631	|Q9BST9|RTKN; Rhotekin	VRAS(0.99)LDSAGGSGSSPILLPTPVVGGPR
1.02	0.01212	|O00515|LAD1; Ladinin-1	LPS(1)VEEAEVPKPLPPASKDEDEDIQSILR
1.01	0.00736	|Q9Y6G9|DC1L1; Cytoplasmic dynein 1 light intermediate chain 1	KPVTVSPTTPTS(1)PTEGEAS
1.00	0.02934	|O60271|JIP4; C-Jun-amino-terminal kinase-interacting protein 4	ERPIS(1)LGIFPLPAGDGLLT(1)PDAQK

Supplemental Table 2. Significantly decreased phosphopeptide abundance in A431/CCKBR cells treated with ^{225}Ac-PP-F11N. MS-based quantification: $\log_2$ ratio > |1| and q < 0.05.

LOG_2 (ratio) ^{225}Ac-PP-F11N /CON	*q*-VALUE	| UniProt |SYMBOL; NAME	SEQUENCE WINDOW POSITION (PROBABILITY>0.75)
-1.00	0.00858	|Q8NCD3|HJURP; Holliday junction recognition protein	GGPAS(1)PGGLQGLETR
-1.01	0.0441	|Q9BVC5|ASHWN; Ashwin	SPSGPVKS(1)PPLSPVGTT(0.85)PVK
-1.01	0.00821	|Q13428|TCOF; Treacle protein	S(1)PQVKPASTMGMGPLGK
-1.01	0.04306	|P56211|ARP19; cAMP-regulated phosphoprotein 19	VTS(1)PEKAEEAK
-1.02	0.01109	|P18887|XRCC1; DNA repair protein XRCC1	TSPVTASDPAGPSYAAATLQASSAASSAS(0.98)PVSR
-1.02	0.01424	|Q14186|TFDP1; Transcription factor Dp-1	VFIDQNLS(1)PGK
-1.02	0.00701	|Q9BQG0|MBB1A; Myb-binding protein 1A	EIPSATQS(0.99)PISK
-1.03	0.01988	|Q86WB0|NIPA; Nuclear-interacting partner of ALK	SQDATFS(1)PGSEQAEK
-1.03	0.01988	|Q86WB0|NIPA;Nuclear-interacting partner of ALK	S(1)PGPIVSR
-1.03	0.02298	|P28749|RBL1; Retinoblastoma-like protein 1	VIAIDSDAES(0.99)PAK
-1.03	0.02058	|Q8WVB6|CTF18; Chromosome transmission fidelity protein 18 homolog	GDAASS(0.98)PAPAASVGSSQGGAR
-1.03	0.01424	|Q9BVC5|ASHWN; Ashwin	KS(0.99)PSGPVKS(1)PPLSPVGTTPVK
-1.03	0.01424	|Q9BVC5|ASHWN; Ashwin	SPSGPVKS(1)PPLS(1)PVGTTPVK
-1.03	0.01921	|P06400|RB; Retinoblastoma-associated protein	TLQTDSIDSFETQRT(1)PR
-1.04	0.04121	|Q9BZQ8|NIBAN; Protein Niban	HNLFEDNMALPSESVSS(0.95)LTDLKPPTGS(0.74)NQAS(0.99)PAR
-1.04	0.02901	|Q9C0C2|TB182; 182 kDa tankyrase-1-binding protein	VNLFPGLS(0.83)PSALK
-1.04	0.04152	|Q14684|RRP1B; Ribosomal RNA processing protein 1 homolog B	VAFDPEQKPLHGVLKT(0.99)PTSS(0.99)PASSPLVAK
-1.04	0.04152	|Q14684|RRP1B; Ribosomal RNA processing protein 1 homolog B	VAFDPEQKPLHGVLKT(0.99)PTSSPASS(0.87)PLVAK
-1.05	0.02855	|Q9Y6D5|BIG2; Brefeldin A-inhibited guanine nucleotide-exchange protein 2	HLDVDLDRQS(0.99)LS(0.90)SIDKNPSER
-1.06	0.03177	|O60684|IMA7; Importin subunit alpha-7	METMAS(1)PGKDNYR
-1.06	0.03463	|P10412|H14; Histone H1.4	SETAPAAPAAPAPAEKT(1)PVKK
-1.07	0.02453	|Q9ULH1|ASAP1; Arf-GAP with SH3 domain, ANK repeat and PH domain-containing protein 1	QEEIDES(1)DDDLDDKPS(1)PIKK
-1.07	0.02453	|Q9ULH1|ASAP1; Arf-GAP with SH3 domain, ANK repeat and PH domain-containing protein 1	QEEIDES(1)DDDLDDKPS(1)PIKK
-1.07	0.03781	|O60890|OPHN1; Oligophrenin-1	S(0.96)PSRPILDGK
-1.07	0.00877	|Q15149|PLEC; Plectin	AQLEPVAS(1)PAK
-1.08	0.00841	|Q9UQ35|SRRM2; Serine/arginine repetitive matrix protein 2	HGGS(1)PQPLATT(0.96)PLSQEPVNPPSEAS(0.77)PTR
-1.08	0.00877	|Q9BTU6|P4K2A; Phosphatidylinositol 4-kinase type 2-alpha	VAAAAGSGPS(1)PPGSPGHDR
-1.09	0.00736	|Q96JM3|CHAP1; Chromosome alignment-maintaining phosphoprotein 1	S(1)PAGS(1)PELR
-1.09	0.00736	|Q96JM3|CHAP1; Chromosome alignment-maintaining phosphoprotein 1	S(1)PAGS(1)PELR
-1.09	0.00736	|Q96JM3|CHAP1; Chromosome alignment-maintaining phosphoprotein 1	KPGPPLS(1)PEIRS(1)PAGS(1)PELR
-1.09	0.01753	|O96028|NSD2; Histone-lysine N-methyltransferase NSD2	IQDPTEDAEAEDT(0.99)PR
-1.09	0.01820	|Q16513|PKN2; Serine/threonine-protein kinase N2	ATSVALPGWS(0.92)PSETR
-1.10	0.01235	|P08559|ODPA; Pyruvate dehydrogenase E1 component subunit alpha, somatic form, mitochondrial	YGMGTS(0.96)VER

-1.10	0.03934	|Q6PL18|ATAD2; ATPase family AAA domain-containing protein 2	LSSAGPRS(1)PYCK
-1.11	0.00877	|O60502|OGA; Protein O-GlcNAcase	S(1)PEMSMQEDCISDIAPMQTDEQTNK
-1.11	0.01066	|Q9ULM3|YETS2; YEATS domain-containing protein 2	ISTASQVSQGTGS(0.99)PVPK
-1.12	0.03677	|Q15717|ELAV1; ELAV-like protein 1	NVALLSQLYHS(1)PAR
-1.12	0.03449	|Q14847|LASP1; LIM and SH3 domain protein 1	GFSVVADT(1)PELQR
-1.13	0.00849	|Q9UIG0|BAZ1B; Tyrosine-protein kinase BAZ1B	SLSGS(1)PLK
-1.13	0.03449	|Q6XZF7|DNMBP; Dynamin-binding protein	HETS(0.81)DHEAEEPDCIISEAPTSPLGHLTS EYDTDR
-1.13	0.00837	|P41229|KDM5C; Lysine-specific demethylase 5C	VQGLLENGDSVTS(0.88)PEK
-1.13	0.04817	|Q8WYP5|ELYS; Protein ELYS	TTSFFLNS(1)PEKEHQEMDEGSQSLEK
-1.14	0.01810	|Q96JM3|CHAP1; Chromosome alignment-maintaining phosphoprotein 1	KPSPSES(0.76)PEPWKPFPAVS(1)PEPR
-1.14	0.00772	|P53985|MOT1; Monocarboxylate transporter 1	EEETS(0.99)IDVAGKPNEVTK
-1.15	0.00636	|A1L390|PKHG3; Pleckstrin homology domain-containing family G member 3	S(1)PLS(1)PTETFSWPDVR
-1.15	0.01995	|Q9Y5K6|CD2AP; CD2-associated protein	FNGGHS(0.99)PTHS(1)PEK
-1.15	0.01995	|Q9Y5K6|CD2AP; CD2-associated protein	FNGGHS(0.99)PTHS(1)PEK
-1.18	0.03673	|Q69YH5|CDCA2; Cell division cycle-associated protein 2	TICTFDSSGFESMS(1)PIKETVSSR
-1.18	0.01988	|Q9ULW0|TPX2; Targeting protein for Xklp2	S(1)PAFALK
-1.20	0.01135	|P13994|CC130; Coiled-coil domain-containing protein 130	QDKPLS(1)PAGSSQEAADTPDTR
-1.20	0.00841	|Q5T200|ZC3HD; Zinc finger CCCH domain-containing protein 13	SKLS(1)PSPSLR
-1.21	0.033	|Q14573|ITPR3; Inositol 1,4,5-trisphosphate receptor type 3	LGFVDVQNCIS(1)R
-1.21	0.01066	|Q8N5I9|CL045; Uncharacterized protein C12orf45	IEVLDS(0.99)PASK
-1.21	0.02322	|Q9ULW0|TPX2; Targeting protein for Xklp2	DPQT(1)PVLQTK
-1.21	0.03287	|Q9Y6G9|DC1L1; Cytoplasmic dynein 1 light intermediate chain 1	SVSSNVASVS(0.99)PIPAGSK
-1.22	0.04433	|P33981|TTK; Dual specificity protein kinase TTK	YVLGQLVGLNS(0.92)PNSILK
-1.22	0.04448	|Q5QJE6|TDIF2; Deoxynucleotidyltransferase terminal-interacting protein 2	QILIACS(1)PVSSVR
-1.22	0.03983	|Q14191|WRN; Werner syndrome ATP-dependent helicase	STEHLSPNDNENDTSYVIES(1)DEDLEMEM LK
-1.22	0.00825	|Q9NRZ9|HELLS; Lymphoid-specific helicase	ETIELS(0.99)PTGRPK
-1.22	0.03390	|Q5SQI0|ATAT; Alpha-tubulin N-acetyltransferase 1	LLLAADPGGS(1)PAQR
-1.24	0.00517	|Q7Z2Z1|TICRR; Treslin	SLLFGAMSEMIS(0.97)PSEK
-1.24	0.00701	|Q12802|AKP13; A-kinase anchor protein 13	ALQLSNS(1)PGASSAFLK
-1.26	0.02606	|P10244|MYBB; Myb-related protein B	TLPFS(0.99)PSQFLNFWNK
-1.26	0.00554	|Q14980|NUMA1; Nuclear mitotic apparatus protein 1	VSLEPHQGPGT(1)PESK
-1.27	0.02145	|Q14160|SCRIB; Protein scribble homolog	MAESPCSPSGQQPPS(1)PPS(1)PDELPANV K
-1.27	0.00749	|Q969E4|TCAL3; Transcription elongation factor A protein-like 3	GTDDS(1)PKDSQEDLQER
-1.28	0.03132	|Q8IXM2|BAP18; Chromatin complexes subunit BAP18	VASGVLS(1)PPPAAPPPSSSSVPEAGGPPIK
-1.28	0.00825	|P51991|ROA3; Heterogeneous nuclear ribonucleoprotein A3	MEVKPPPGRPQPDS(1)GR
-1.28	0.01988	|Q9BVJ6|UT14A; U3 small nucleolar RNA-associated protein 14 homolog A	EQMIDLQNLLTT(0.75)QSPSVK
-1.29	0.02501	|Q6PGN9|PSRC1; Proline/serine-rich coiled-coil protein 1	LS(1)LGPLS(1)PEKLEEILDEANR
-1.29	0.02501	|Q6PGN9|PSRC1; Proline/serine-rich coiled-coil protein 1	LS(1)LGPLS(1)PEKLEEILDEANR
-1.29	0.01820	|Q7L2J0|MEPCE; 7SK snRNA methylphosphate capping enzyme	DITDPLSLNTCTDEGHVVLAS(1)PLK
-1.29	0.00655	|Q92797|SYMPK; Symplekin	EERS(1)PQTLAPVGEDAMK
-1.31	0.00311	|Q6ZSR9|YJ005; Uncharacterized protein FLJ45252	LGGAVPFAPPEVS(1)PEQAK

-1.31	0.00821	|P00533|EGFR; Epidermal growth factor receptor	GSHQIS(1)LDNPDYQQDFFPK
-1.31	0.01129	|P41002|CCNF; Cyclin-F	SCLQCRPPS(1)PPESSVPQQQVK
-1.32	0.03177	|Q08945|SSRP1; FACT complex subunit SSRP1	QLSES(1)FK
-1.33	0.02288	|Q9NYF8|BCLF1; Bcl-2-associated transcription factor 1	EEEWDPEYT(1)PK
-1.33	0.02288	|Q9Y2W1|TR150; Thyroid hormone receptor-associated protein 3	NREEEWDPEYT(1)PK
-1.33	0.00636	|Q14181|DPOA2; DNA polymerase alpha subunit B	AIST(0.99)PETPLTK
-1.33	0.02611	|P35568|IRS1; Insulin receptor substrate 1	VNLS(1)PNR
-1.33	0.03680	|P16402|H13; Histone H1.3	SETAPLAPTIPAPAEKT(1)PVK
-1.34	0.01206	|Q96JM3|CHAP1; Chromosome alignment-maintaining phosphoprotein 1	KPSGS(0.99)PDLWKLS(1)PDQR
-1.34	0.01206	|Q96JM3|CHAP1; Chromosome alignment-maintaining phosphoprotein 1	KPSGS(0.99)PDLWKLS(1)PDQR
-1.34	0.01066	|Q66K74|MAP1S; Microtubule-associated protein 1S	S(1)AS(1)PHDVDLCLVSPCEFEHR
-1.35	0.02613	|O75152|ZC11A; Zinc finger CCCH domain-containing protein 11A	KVEAPETNIDKT(1)PK
-1.39	0.00144	|Q8IWS0|PHF6; PHD finger protein 6	TAHNSEADLEES(1)FNEHELEPSS(0.91)PK
-1.41	0.04391	|O43399|TPD54; Tumor protein D54	NSATFKS(1)FEDR
-1.42	0.00588	|O95297|MPZL1; Myelin protein zero-like protein 1	DYTGCSTSESLS(0.99)PVK
-1.42	0.00548	|P78347|GTF2I; General transcription factor II-I	TNT(1)PVKEDWNVR
-1.43	0.00517	|P49792|RBP2; E3 SUMO-protein ligase RanBP2	SALS(0.99)PSKS(1)PAK
-1.43	0.00517	|P49792|RBP2; E3 SUMO-protein ligase RanBP2	SALS(0.99)PSKS(1)PAK
-1.43	0.00643	|P21359|NF1; Neurofibromin	GSEGYLAATYPTVGQT(0.85)SPR
-1.43	0.02610	|P55327|TPD52; Tumor protein D52	NSPTFKS(1)FEEK
-1.43	0.03719	|P00533|EGFR; Epidermal growth factor receptor	DPHYQDPHSTAVGNPEY(1)LNTVQPTCVN STFDSPAHWAQK
-1.44	0.03328	|Q69YH5|CDCA2; Cell division cycle-associated protein 2	GENLENIEPLQVSFAVLSS(0.98)PNK
-1.49	0.00640	|Q9NVP2|ASF1B; Histone chaperone ASF1B	LEAIETQDPSLGCGLPLNCT(1)PIK
-1.50	0.00695	|O76021|RL1D1; Ribosomal L1 domain-containing protein 1	FFTT(0.88)PSK
-1.52	0.00342	|Q53F19|NCBP3; Nuclear cap-binding protein subunit 3	MISTPS(0.99)PK
-1.52	0.00128	|Q8IWS0|PHF6; PHD finger protein 6	TAHNSEADLEESFNEHELEPSS(0.99)PK
-1.54	0.01631	|O60341|KDM1A; Lysine-specific histone demethylase 1A	ASPPGGLAEPPGSAGPQAGPTVVPGSATP METGIAET(0.99)PEGR
-1.54	0.00164	|Q15648|MED1; Mediator of RNA polymerase II transcription subunit 1	LAS(1)PMKPVPGT(0.94)PPSSK
-1.54	0.00164	|Q15648|MED1; Mediator of RNA polymerase II transcription subunit 1	LAS(1)PMKPVPGT(0.98)PPSSK
-1.55	0.01852	|Q14684|RRP1B; Ribosomal RNA processing protein 1 homolog B	VAFDPEQKPLHGVLKT(0.99)PTSS(0.99)PA SSPLVAK
-1.55	0.00296	|Q9H2D6|TARA; TRIO and F-actin-binding protein	QALDYVELSPLTQAS(1)PQR
-1.55	0.00277	|Q01082|SPTB2; Spectrin beta chain, non-erythrocytic 1	AQTLPTSVVTITSES(0.82)SPGKR
-1.56	0.01135	|P18887|XRCC1; DNA repair protein XRCC1	KT(0.98)PSKPPAQLS(0.99)PSVPK
-1.56	0.00216	|P17096|HMGA1; High mobility group protein HMG-I/HMG-Y	EPSEVPT(1)PK
-1.57	0.00112	|Q6MZP7|LIN54; Protein lin-54 homolog	IAIS(1)PLKS(1)PNK
-1.57	0.00112	|Q6MZP7|LIN54; Protein lin-54 homolog	IAIS(1)PLKS(1)PNK
-1.58	0.00213	|Q12888|TP53B; Tumor suppressor p53-binding protein 1	EQLSAQELMESGLQIQKS(1)PEPEVLSTQE DLFDQSNK
-1.59	0.00087	|P43487|RANG; Ran-specific GTPase-activating protein	DTHEDHDTS(0.99)TENTDESNHDPQFEPIV SLPEQEIK
-1.59	0.01109	|P08729|K2C7; Keratin, type II cytoskeletal 7	SIHFSS(0.99)PVFTSR
-1.60	0.00610	|Q14684|RRP1B; Ribosomal RNA processing protein 1 homolog B	VAFDPEQKPLHGVLKT(0.99)PTSSPASS(0. 87)PLVAK

-1.60	0.00610	|Q14684|RRP1B; Ribosomal RNA processing protein 1 homolog B	VAFDPEQKPLHGVLKT(0.99)PTSS(0.90)PASS(0.99)PLVAK
-1.60	0.00131	|Q9UJX2|CDC23; Cell division cycle protein 23 homolog	RVS(1)PLNLSSVT(1)P
-1.60	0.00131	|Q9UJX2|CDC23; Cell division cycle protein 23 homolog	RVS(1)PLNLSSVT(1)P
-1.60	0.00144	|P22234|PUR6; Multifunctional protein ADE2	EVYELLDS(1)PGK
-1.61	0.00610	|Q96Q89|KI20B; Kinesin-like protein KIF20B	FGDFLQHS(0.99)PSILQSK
-1.64	0.01695	|Q5VUA4|ZN318; Zinc finger protein 318	ISAPELLLHS(1)PAR
-1.65	0.01806	|O75475|PSIP1; PC4 and SFRS1-interacting protein	AVDITT(0.78)PK
-1.65	0.01372	|P07948|LYN; Tyrosine-protein kinase Lyn	AEERPTFDYLQSVLDDFYTATEGQY(1)QQQP
-1.65	0.01248	|P35251|RFC1; Replication factor C subunit 1	IGEVSS(0.75)PK
-1.66	0.00476	|Q99638|RAD9A; Cell cycle checkpoint control protein RAD9A	DSLLDGHFVLATLSDTDSHS(1)QDLGS(1)PER
-1.66	0.01129	|Q9UKM9|RALY; RNA-binding protein Raly	TRDDGDEEGLLTHSEEELEHSQDT(0.77)DADDGALQ
-1.67	0.00572	|Q13330|MTA1; Metastasis-associated protein MTA1	VAPVINNGS(0.99)PTILGK
-1.67	0.00115	|Q9BYG3|MK67I; MKI67 FHA domain-interacting nucleolar phosphoprotein	TVDSQGPT(1)PVCT(1)PTFLER
-1.67	0.00115	|Q9BYG3|MK67I; MKI67 FHA domain-interacting nucleolar phosphoprotein	TVDSQGPT(1)PVCT(0.99)PTFLER
-1.68	0.00131	|Q9NR30|DDX21; Nucleolar RNA helicase 2	KAEPSEVDMNS(1)PK
-1.70	0.01206	|Q86YP4|P66A; Transcriptional repressor p66-alpha	GTTATSAQANSTPTSVASVVTSAES(0.92)PASR
-1.71	0.03915	|Q9NWH9|SLTM; SAFB-like transcription modulator	QAIEEEGGDPDNIELTVSTDT(0.81)PNKKPTK
-1.71	0.01109	|Q99504|EYA3; Eyes absent homolog 3	LSSGDPSTSPSLSQTT(0.88)PSKDTDDQSR
-1.73	0.00115	|Q96JM3|CHAP1; Chromosome alignment-maintaining phosphoprotein 1	PAPSVS(1)PGPWKPIPSVS(1)PGPWKPTPSVSSASWK
-1.73	0.00115	|Q96JM3|CHAP1; Chromosome alignment-maintaining phosphoprotein 1	PAPSVS(1)PGPWKPIPSVS(1)PGPWKPTPSVSSASWK
-1.74	0.00164	|Q9H211|CDT1; DNA replication factor Cdt1	LACRT(1)PS(1)PARPALR
-1.74	0.00164	|Q9H211|CDT1; DNA replication factor Cdt1	LACRT(1)PS(1)PARPALR
-1.78	0.01698	|Q86YP4|P66A; Transcriptional repressor p66-alpha	GVLHTFS(0.99)PSPK
-1.79	0.00131	|P11388|TOP2A; DNA topoisomerase 2-alpha	TQMAEVLPS(1)PR
-1.80	0.01135	|Q92614|MY18A; Unconventional myosin-XVIIIa	VASGSDLHLTDIDS(0.92)DSNR
-1.84	0.00080	|Q12834|CDC20; Cell division cycle protein 20 homolog	EAAGPAPS(1)PMR
-1.87	0.00175	|Q9UKM9|RALY; RNA-binding protein Raly	TRDDGDEEGLLTHS(1)EEELEHSQDTDADDGALQ
-1.94	0.03692	|P27816|MAP4; Microtubule-associated protein 4	DGVLTLANNVT(1)PAKDVPPLSETEATPVPIK
-1.94	0.00841	|P49792|RBP2; E3 SUMO-protein ligase RanBP2	NLFASFPTEESSINYTFKT(1)PEK
-1.96	0.01235	|Q9NQ88|TIGAR; Fructose-2,6-bisphosphatase TIGAR	EQFS(0.92)QGSPSNCLETSLAEIFPLGK
-2.02	0.00932	|Q14978|NOLC1; Nucleolar and coiled-body phosphoprotein 1	VAGGAAPSKPAS(0.95)AK
-2.10	0.01154	|P06748|NPM; Nucleophosmin	MQAS(1)IEK
-2.16	0.01631	|P19338|NUCL; Nucleolin	VAVAT(1)PAK
-2.17	0.00399	|Q9NQS7|INCE; Inner centromere protein	HS(1)PIAPSS(0.92)PSPQVLAQK
-2.23	0.00199	|Q9H1E3|NUCKS; Nuclear ubiquitous casein and cyclin-dependent kinase substrate 1	ATVT(0.99)PS(1)PVKGK
-2.23	0.00199	|Q9H1E3|NUCKS; Nuclear ubiquitous casein and cyclin-dependent kinase substrate 1	ATVT(0.99)PS(1)PVKGK
-2.23	0.00131	|Q14978|NOLC1; Nucleolar and coiled-body phosphoprotein 1	S(1)PAVKPAAAPK
-2.49	0.00399	|O60318|GANP; Germinal-center associated nuclear protein	KPGDGEVSPSTEDAPFQHS(1)PLGK

-2.50	0.00021	|P78332|RBM6; RNA-binding protein 6	EGETQGVAFEHESPADFQNS(1)QS(1)PVQ DQDK
-2.84	0.00277	|Q14978|NOLC1; Nucleolar and coiled-body phosphoprotein 1	VADNS(1)FDAK
-3.51	0.00013	|Q14978|NOLC1; Nucleolar and coiled-body phosphoprotein 1	LQT(1)PNT(1)FPK
-3.51	0.00013	|Q14978|NOLC1; Nucleolar and coiled-body phosphoprotein 1	LQT(1)PNT(1)FPK
-3.53	0.00017	|P18887|XRCC1; DNA repair protein XRCC1	KT(0.98)PSKPPAQLS(0.99)PSVPK
-3.53	0.00017	|P18887|XRCC1; DNA repair protein XRCC1	KT(0.98)PSKPPAQLS(0.99)PSVPK

Supplemental Table 3. Significant changes in relative total protein abundance levels after ^{225}Ac-PP-F11N treatment in A431/CCKBR cells. MS-based quantification shown as $\log_2$ ratio, $q < 0.05$.

LOG_2 RATIO: ^{225}Ac-PP-F11N/CON	***q*-value**	**UniProt**	**PROTEIN**
1.54	0.0186	|Q9H8M7|F188A_HUMAN	Ubiquitin carboxyl-terminal hydrolase MINDY-3
1.10	0.0496	|P47974|TISD_HUMAN	mRNA decay activator protein ZFP36L2
-1.65	0.0192	|Q96S97|MYADM_HUMAN	Myeloid-associated differentiation marker

Supplemental Table 4. Significantly enriched (*P*<0.01) biological processes and signal transduction pathways in response to ^{225}Ac-PP-F11N treatment.

^{225}Ac-PP-F11N	Fold En.	*P-value*
RNA transcription and processing		
Regulation of transcription from RNA polymerase II promoter (BRCA1, FOSL1, HTATSF1, JUND, LRRFIP1, RBBP8, RB1, RBL1, SLTM, SNW1, CHD4, FOXK1, GTF2I, KDM1A, MAPK14, NUCKS1, TCEAL3,TFDP1) GOTERM_BP	3.0	1.0E-4
Transcription, DNA-template (ATAD2, BCLAF1, BRCA1, EYA3, GATAD2A, HTATSF1, LRRFIP1, MYBBP1A, PSIP1, PHF6, RALY, RB1, RBL1, SLTM, SP110, WHSC1, ADNP, ASF1B, BAZ1B, CBX3, CHD4, DNTTIP2,FOXK1, HELLS, HDAC9, LIN54, KDM1A, KDM5C, MTA1, MAPK14, PNN, PKN2, RFC1, TCEAL3, TFDP1, TP53BP1, TP53, UIMC1, ZMYND11, ZNF280C, ZNF318, ZNF83) GOTERM_BP	1.6	2.6E-3
mRNA splicing, via spliceosome (ELAVL1, HTATSF1, RALY, SNW1, YBX1, HNRNPA3, HNRNPU, METTL3, PNN, PABPN1, SRRM2, SRRT) GOTERM_BP	4.0	2.2E-4
Regulation of mRNA stability (ELAVL1, SERBP1, SET, ZFP36L2, ZFP36, PSMD4, PSMA5) GOTERM_BP	5.0	2.7E-3
mRNA transport (AHCTF1, ZFP36, HNRNPA3, MCM3AP, NCBP3) GOTERM_BP	7.9	3.6E-3
Cell morphology, adhesion, and phenotype		
Cell-cell adhesion (AHNAK, ASAP1, LASP1, LRRFIP1, NUMB, PPFIBP1, RANBP1, SERBP1, WASF2, ADD1, CAST, LAD1, PAICS, PLEC, PKN2, RSL1D1, SPTBN1, TNKS1BP1, TJP1) GOTERM_BP	5.2	2.9E-8
Transport and protein modifications		
Protein sumoylation (BRCA1, RANBP2, WRN, INCENP, MDC1, MTA1, NUP35, SMC1A, TOP2A, TRIM28, TP53BP1, TP53) GOTERM_BP	7.6	5.1E-7
Positive regulation of glucose import (ARPP19, IRS1, IRS2, MAPK14) GOTERM_BP	9.9	7.5E-3

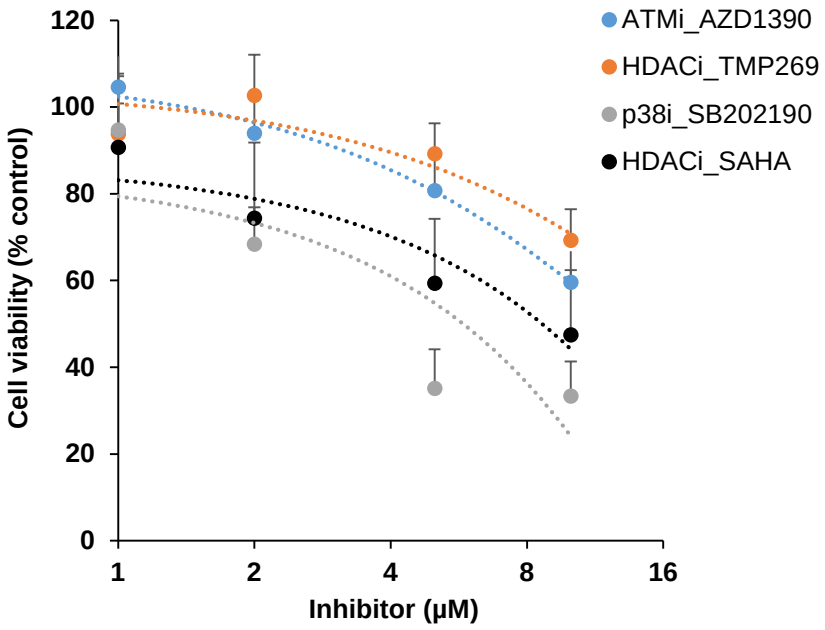

Supplemental Figure 1. Viability analysis in ATM, HDAC, and p38 inhibitor-treated cells. Viability of A431/CCKBR cells 24 h after incubation with 1, 2, 5, and 10 μM of AZD1390, TMP269, SB202190, and SAHA. Results are shown as % viability compared with control cells.

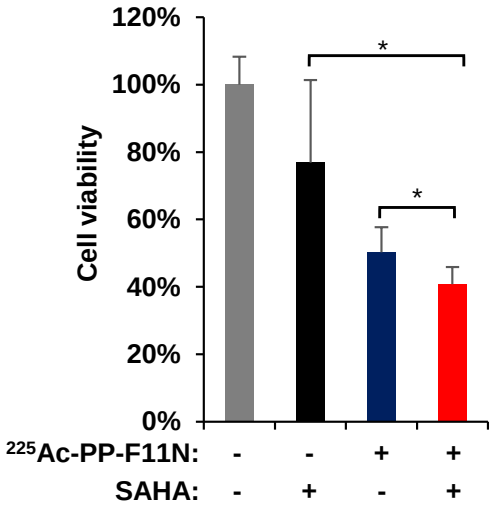

Supplemental Figure 2. Treatment with HDAC inhibitor SAHA sensitizes A431/CCKBR cells to ^{225}Ac-PP-F11N. Cell viability 24 h after treatment with 3 kBq/ml 225Ac-PP-F11N or 2 µM SAHA alone or in combination ^{225}Ac-PP-F11N. Bars represent mean ± SD. *$p < 0.05$.

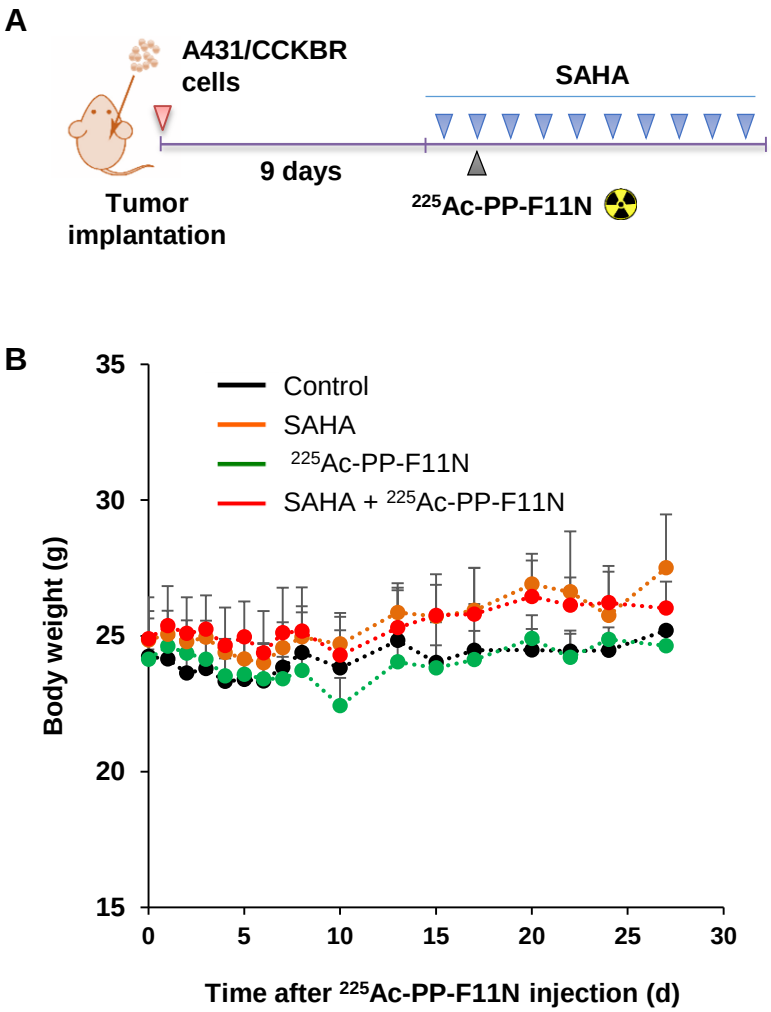

Supplemental Figure 3. Body weight of A431/CCKBR-tumor bearing nude mice during PRRT with radiolabeled minigastrin and HDAC inhibitor SAHA. (A) Schematic representation of the treatment. (B) Body weight of control and treated mice with 30 kBq ^{225}Ac-PP-F11N alone or in combination with 10 doses of 50 mg/kg SAHA administrated daily. Values represent mean ± SD.

Supplemental Material and Methods

Radiolabeling

For radiolabeling, 60 nmol of PP-F11N and 6 MBq ^{225}Ac (12 pmol) were combined in 0.4 M ammonium acetate buffer (pH 5.5) supplemented with 21 µL of 0.5 M sodium ascorbate to a total volume of 510 µL and the reaction was carried out at 75 °C for 1 h. After labeling, 2 µL of 0.5 mM EDTA in metal-free water was added, and radiolabeled ^{225}Ac-PP-F11N was separated from the unlabeled PP-F11N and free radionuclides using Merck Hitachi LaChrom 2D high-performance liquid chromatography (HPLC) system as previously described (*6*). The purified ^{225}Ac-PP-F11N with the specific activity of 475 MBq/nmol was concentrated on SpeedVac and diluted in PBS prior *in vitro* and *in vivo* experiments.

Cell Culture and Proliferation Assay

A431/CCKBR cells were cultivated in Dulbecco's Modified Eagle Medium (DMEM) with 10% (v/v) fetal bovine serum, 2 mM glutamine, 0.1 mg/mL streptomycin, 100 IU/mL penicillin and 1.25 g/mL fungizone (BioConcept) in a humidified incubator with 5% CO_2 at 37°C. For proliferation assay, 4 x 10^3 cells in 150 µL medium were seeded on 96-well plates. Next day, cells were treated with 1-3 kBq/mL ^{225}Ac-PP-F11N for 2 h, and the medium containing ^{225}Ac-PP-F11N was replaced with 100 µL fresh medium with or without 2, 5, or 10 µM inhibitors, as indicated. After 24 or 48 h, cell proliferation was analyzed by using the CellTiter 96 AQueous Non-Radioactive Cell Proliferation Kit (Promega) according to the manufacturer's instruction and absorbance at 570nm with a reference of 650nm was measured using a MicroPlate Reader (PerkinElmer). The absorbance of the untreated control was set to 100% of cell viability. Each assay was performed in triplicates.

Preparation of Tryptic Peptides and Phosphopeptide Enrichment

A431/CCKBR cells were grown on 150 mm TC plates and 100% confluent cells were treated with 10 kBq/mL ^{225}Ac-PP-F11N for 2 h. Control plates were incubated with medium without radiolabeled compound. After incubation time, control and treated cells were washed with PBS, and incubated with normal growth medium for another 2 h. The total protein lysates were prepared in 8 M urea lysis buffer in 0.1 M Ambic supplemented with cOmplete mini protease and PhosSTOP phosphatase inhibitors (Roche). For each sample, 500 µg of proteins were taken and used for on-filter digestion using an adaptation of the filter-aided sample preparation (FASP) protocol. Briefly, proteins were diluted in 200 µL of UT buffer (8 M Urea in 100 mM Tris/HCL, pH 8.2), loaded on Ultracel 30000 MWCO centrifugal unit (Amicon Ultra, Merck, Darmstadt, Germany) and centrifuged at 14000 g. SDS buffer was exchanged by one centrifugation round of 200 µL UT buffer. Alkylation of reduced proteins was carried by 5 min incubation with 100 µL iodoacetamide 0.05 M in UT buffer, followed by three 100 µL washing steps with UT and two 100 µL washing steps with Triethylammonium bicarbonate buffer (TEAB, pH 8). Finally, proteins were on-filter digested using 120 µL of 0.05 TEAB (pH 8) containing trypsin (Promega, Madison, WI, USA) in a ratio 1:50 (w/w). Digestion was performed overnight in a wet chamber at room temperature, and peptides were eluted by centrifugation at 14000 g for 20 minutes. After elution, 5 µL of peptide mixtures were taken and stored for later MS analysis of the proteomes. The remaining volume was dried almost to completeness for enrichment of the phosphopeptides by using a KingFisher Flex System (Thermo Fisher Scientific) and MagReSyn Ti-IMAC beads (ReSyn Biosciences, Gauteng, South Africa). Beads were conditioned following the manufacturer's instructions, consisting of 2 washes with 200 µL of 70% ethanol, 1 wash with 100 µL of 1 M NH_4OH and 3 washes with loading buffer (0.1 M glycolic acid in 80% ACN, 5% trifluoroacetic acid (TFA)). Samples were diluted with 200 µL of loading buffer. The beads, wash solutions and the samples were loaded into 96 deep well plates and transferred to the KingFisher. The protocol of the robot carried out the following steps: washing of the magnetic beads in loading buffer (5 min), binding

of the phosphopeptides to the beads (20 min), washing the beads in wash 1 (0.1 M glycolic acid in 80% ACN, 5% TFA, 2 min), wash 2 (80% ACN, 1% TFA, 2 min), wash 3 (10% ACN, 0.2% TFA, 2 min) and eluting the phosphopeptides from the magnetic beads (1 M NH_4OH, 10 min). The phosphopeptides were dried to the completeness and re-solubilized with 10 µL of 3% acetonitrile, 0.1% formic acid for MS analysis. 1 µL of iRT peptides (Biognosys) at 1:100 dilution were added to each samples.

Liquid Chromatography-Mass Spectrometry Analysis

The analysis of phosphoproteomics sample was performed on a Q Exactive HF mass spectrometer (Thermo Scientific) equipped with a Digital PicoView source (New Objective) and coupled to an M-Class UPLC (Waters). Solvent composition at the two channels was 0.1% formic acid for channel A and 0.1% formic acid, 99.9% acetonitrile for channel B. Column temperature was 50 °C. For each sample 4 µL of peptides were loaded on a commercial ACQUITY UPLC M-Class Symmetry C18 Trap Column (100Å, 5 µm, 180 µm x 20 mm, Waters) followed by ACQUITY UPLC M-Class HSS T3 Column (100Å, 1.8 µm, 75 µm X 250 mm, Waters). The peptides were eluted at a flow rate of 300 nL/min by a gradient from 5 to 40% B in 90 min. The column was cleaned after the run by increasing to 98% B and holding 95% B for 10 min prior to re-establishing the loading condition. Samples were acquired in a randomized order. The mass spectrometer was operated in data-dependent mode (DDA), acquiring a full-scan MS spectra (350−1’500 m/z) at a resolution of 120’000 at 200 m/z after accumulation to a target value of 3’000’000, and a maximum injection time of 50 ms followed by HCD (higher-energy collision dissociation) fragmentation on the ten most intense signals per cycle. HCD spectra were acquired at a resolution of 60’000 using a normalized collision energy of 25 and a maximum injection time of 120 ms. The automatic gain control (AGC) was set to 1’000’000 ions. Charge state screening was enabled. Singly, unassigned, and charge states higher than eight were rejected. Only precursors with intensity above 100’000 were selected for MS/MS. Precursor masses previously selected for

MS/MS measurement were excluded from further selection for 30 s, and the exclusion window was set at 10 ppm. The samples were acquired using internal lock mass calibration on m/z 371.1012 and 445.1200. MS analysis of the proteome samples was performed right after the acquisition of the phosphoproteomics data, on the same Q Exactive HF mass spectrometer, using the same UPLC conditions as of the phosphoproteomics experiment. Samples were dried and re-solubilized with 15 µL of 3% acetonitrile, 0.1% formic acid for MS analysis. 1 µL of iRT peptides (Biognosys) at 1:100 dilution was added to each sample. Two microliters were injected. The MS method changed only for the following parameters: HCD fragmentation was performed on the twelve most intense signals per cycle. HCD spectra were acquired at a resolution of 30'000 using a normalized collision energy of 28 and a maximum injection time of 50 ms. The automatic gain control (AGC) was set to 100'000 ions. The MS proteomics data were handled using the local laboratory information management system (LIMS) and all relevant data have been deposited to the ProteomeXchange Consortium via the PRIDE (http://www.ebi.ac.uk/pride) partner repository (*9*).

Protein and Phosphopeptide Identification and Label-Free Quantification

The acquired raw MS data were processed by MaxQuant (version 1.6.2.3), followed by protein identification using the integrated Andromeda search engine. Spectra were searched against a canonical Uniprot reference proteome of Homo sapiens (UP000005640, version 2016-12-09), concatenated to common protein contaminants. Carbamidomethylation of cysteine was set as a fixed modification, while methionine oxidation and N-terminal protein acetylation were set as a variable. Additionally, serine, threonine, and tyrosine phosphorylation were set as variable modifications in the search for the phosphoproteome. Enzyme specificity was set to trypsin/P allowing a minimal peptide length of 7 amino acids and a maximum of two missed cleavages. MaxQuant Orbitrap default search settings were used. The maximum false discovery rate was set to 0.01 for peptides and 0.05 for proteins. Label-free quantification was enabled and a 2

minutes window for the match between runs was applied. In the MaxQuant experimental design template, each file is kept separate in the experimental design to obtain individual quantitative values. Statistics of the phosphopeptide analysis and the total proteome analysis were merged and the calculated p-values were adjusted for multiple testing (*q*-values). Values of $q < 0.05$ were considered statistically significant.

Bioinformatics

DAVID bioinformatics platform was used to annotate the function of the protein groups identified by phosphoproteomics and proteomics analysis (https://david.ncifcrf.gov/). The proteins, which contain peptides with significantly altered phosphorylation or total protein level after ^{225}Ac-PP-F11N treatment were categorized based on their involvement in biological processes (GOTERM_BP) or signal transduction pathways (BIOCARTA) by using the Gene Ontology annotation tool. STRING 11.1 protein-protein interaction database (http://string-db.org/) was used to visualize the networks of proteins, which phosphorylation or protein level was changed in response to ^{225}Ac-PP-F11N treatment. Present protein-protein associations were based on evidence with high confidence (interaction score > 0.7).

Western Blot

A431/CCKBR cells were treated with 6 kBq/mL ^{225}Ac-PP-F11N (2h internalization time) alone or in combination with 1 or 10 µM inhibitors for 2 h. Total protein lysates were prepared in lysis buffer containing 50 mM Tris-HCl pH 7.5, 150 mM NaCl, 1% Triton X, 0.1% SDS with 1 mM sodium orthovanadate, 1 mM NaF and protease inhibitor cocktail (Roche). Antibodies against phospho-P53 S15 (16G8), phospho-H2A.X S139 (2577), and GAPDH (14C10) were from Cell Signaling Technology (CST), whereas phospho-53BP1 S1778 (PA5-17462) was from EnoGene, and phospho-HDAC9/4/5 S246/S259/S220 (SAB4300269) was from Sigma-Aldrich. Secondary anti-

rabbit and anti-mouse HRP-linked antibodies were from CST and the standard WB experiments were performed as described previously (*11*).

Immunocytochemistry

3 x 10^4 cells per well were seeded on an 8-well chamber slide (iBidi). On the next day, cells were treated with 3 kBq/ml ^{225}Ac-PP-F11N alone or in combination with 2 µM SAHA, as described above. After 24 h incubation, the PBS-washed cells were fixed in 4 % paraformaldehyde/ PBS and used for immunohistochemistry. Cells were first permeabilized with 1% NP40/PBS for 5 minutes and then blocked with a blocking buffer (1% BSA/ 0.3% Triton X-100/ PBS) for 1 hour. Cells were then incubated overnight at 4°C with 1:1000 diluted rabbit anti-phospho-histone H2A.X (Ser139) antibody (CST, #2577), washed three times with PBS, and then incubated with a Cy3-labeled donkey anti-rabbit antibody (Jackson ImmunoResearch). Nuclei were stained by incubating for 10 minutes in 1 µg/ml Hoechst 33258/ PBS. Images were collected on a Leica Stellaris confocal microscope with a 20x objective. Single sections with a resolution of 4096x4096 pixels were acquired. Images were analyzed with a CellProfiler pipeline as described by CellProfiler developers (https://cellprofiler.org/examples). Signals from 150–400 cell nuclei were counted for each condition. For statistical analysis one-way ANOVA followed by Tukey's multiple comparison tests were performed using GraphPad Prism 7.00 for Windows 10.